

# Galaxy rotation curves using a non-parametric regression method: core, cusp and fuzzy scalar field dark matter models

Lizbeth M. Fernández-Hernández,<sup>1\*</sup> Ariadna Montiel,<sup>2†</sup> Mario A. Rodríguez-Meza<sup>1‡</sup>

<sup>1</sup>*Departamento de Física, Instituto Nacional de Investigaciones Nucleares, AP 18-1027, Ciudad de México 11801, México*

<sup>2</sup>*Instituto de Ciencias Físicas, Universidad Nacional Autónoma de México, 62210, Cuernavaca, Morelos, México*

Accepted XXX. Received YYY; in original form ZZZ

## ABSTRACT

We present a non-parametric reconstruction of the rotation curves (RC) for 88 spiral galaxies under the LOESS+SIMEX technique. In order to compare methods we also perform the parametric approach assuming core and cuspy dark matter (DM) profiles: PISO, NFW, Burkert, Spano, the soliton and two fuzzy soliton+NFW. As result of this two approaches, a comparison of the RC obtained is carried out by computing the distance between central curves and the distance between  $1\sigma$  error bands. Furthermore, we perform a model selection according to two statistical criteria, the BIC and the value of  $\chi^2_{red}$ . We work with two groups. The first one is a comparison between PISO, NFW, Spano and Burkert showing that Spano is the most favored model satisfying our selection criteria. For the second group we select soliton, NFW and Fuzzy models, resulting the soliton as the best model. Moreover according to the statistical tools and non-parametric reconstruction we are able to classify galaxies as core or cusp. Finally, using an MCMC method, we compute for each of the DM models the characteristic surface density,  $\mu_{DM} = \rho_s r_s$ , and the mass within 300 pc. We found that there is a common mass for spiral galaxies of the order of  $10^7 M_\odot$ , which is in agreement with results for dSph Milky Way satellites, independent of the model. This result is also consistent with our finding that there is a constant characteristic volume density of haloes. Finally, we also find that  $\mu_{DM}$  is not constant, which is in tension with previous literature.

**Key words:** galaxy rotation curve – dark matter – fuzzy scalar field dark matter

## 1 INTRODUCTION

Since the observation of the rotation curves in spiral galaxies (Sofue & Rubin (2001)) one of the main problems in galactic dynamics is how to determine the shape of the dark matter halo. Currently, a variety of dark matter density profiles can be found in the literature, e.g. Begeman et al. (1991); Navarro et al. (1996); Burkert (1995); Spano et al. (2008); Einasto (1965); García-Aspeitia et al. (2017); Chen et al. (2017); Hernández-Almada & García-Aspeitia (2018)).

When used in  $N$ -body simulations, some of these models are able to reproduce the large scale structure of the universe. Nevertheless, at smaller scales, some problems arise such as the DM content in dwarf galaxies or the number of satellite galaxies, these problems are expected to be

strongly related to the baryonic contribution to the dynamics of structure formation. On the other hand, there is the so called cusp-core problem consisting in the observation that in some galaxies the center of the dark matter halo features a core behavior  $\rho_{DM} \sim \text{constant}$ , which is in disagreement with the cuspy behavior predicted by the simulations,  $\rho_{DM} \sim r^{-1}$  (for review see: de Blok (2010); Pontzen & Governato (2014)). Furthermore, by cosmological simulations Schive et al. (2014), a density profile with inner soliton-like profile was derived, called Fuzzy, wave or ultra-light axion with an asymptotic NFW declination in the outer points, see Bernal et al. (2018) and references therein for a review.

It would be a step forward toward to the solution of the cusp-core problem, if we had data of galaxy rotation curves with higher spatial resolution at the center of the system. This later was one of the main concerns of the Spitzer Photometry and Accurate Rotation Curves (SPARC) database team (Lelli et al. 2016). They probed the inner regions at high spatial resolutions, and classify galaxies using a qual-

\* E-mail: lfernandez@fis.cinvestav.mx

† E-mail: amontiel@icf.unam.mx

‡ E-mail: marioalberto.rodriguez@inin.gob.mx

ity flag  $Q$ : 1 = high, 2 = medium and 3 = low. With more accurate data we may be able to fit core models and on the contrary, with low resolution data the cusp models, like the NFW (de Blok & Bosma 2002; Oh et al. 2015).

On the other hand, in the standard approach one selects a particular density profile or model of rotation curves, with a specific functional form between dependent and independent variables and then constrain the parameters of the chosen theory employing bayesian methods together observational data of galaxies (Bernal et al. 2018; Garcia-Aspeitia et al. 2017; Li et al. 2019). The main problem of this method is the susceptibility to bias if the data is not well-represented by the assumed parametric model. Since the goal is to determine the best-fit of the model parameters, this approach is called parametric.

In contrast, the goal of a *non-parametric* approach is to infer a global trend directly from data to assess sensitivity about the assumptions made in an specific parametric model and try to distinguish among competing cosmological models, for instance. Besides, it is also useful if a well justified functional form for the object of interest is not available or, even with a reasonable parametric model but there is a lack of data to infer other details of the theory. Specifically, in this kind of scenarios a correlation between each data point is assumed but prior information about the functional form of the observable is not required. So far it has been possible to gain useful information about the dark energy cosmic evolution directly from observations by using this kind of non-parametric methods, see for instance Huterer & Starkman (2003); Espana-Bonet & Ruiz-Lapuente (2005); Bonvin et al. (2006); Shafieloo et al. (2006); Bogdanos & Nesseris (2009); Holsclaw et al. (2010); Alberto Vazquez et al. (2012); Montiel et al. (2014).

In this work, the approach LOESS+SIMEX presented in Montiel et al. (2014), which is a simple but powerful non-parametric regression technique that takes into account the observational errors, is employed. LOESS (Locally Weighted Scatterplot Smoothing) method originally was introduced in Cleveland (1979) and further developed in Cleveland & Devlin (1988). It recovers the global trend of data by using a weighted least squares and fitting a low-degree polynomial to a subset of the data, giving more weight to points near the point whose response is being estimated and less weight to points further away. Because LOESS method does not take into account the measurement errors while reconstructing the response parameter, the effect of observational errors should be captured with another statistical technique: the SIMEX (Simulation and Extrapolation) method (Cook & Stefanski 1994; Stefanski & Cook 1995). These methods were first used together in cosmology in Montiel et al. (2014) with significant success. Later on, this technique was applied for reconstructing other cosmological quantities in Rani et al. (2015); Rana et al. (2016); Escamilla-Rivera & Fabris (2016) providing also good results. Here we adapt the method to reconstruct the rotation curves of galaxies without assuming any prior or DM model.

We investigate the influence of the galactic DM halo on the rotation curves applying the LOESS+SIMEX method, for which the galaxy rotation curves from the SPARC database (Lelli et al. 2016) are used, in particular a subsample whose main feature is that the contribution of dark matter is greater than 50% such that the structure of the

rotation curve comes mostly from dark matter and not from baryonic information (gas and stars). Another important characteristic of the subsample is that we only consider those galaxies with a quality factor of  $Q = 1$  or 2, according to Lelli et al. (2016).

Furthermore, it is presented a comparison of the  $\chi^2$  fitted velocity rotation curves with the non-parametric reconstruction method through the distance between central curves ( $B_{DIST}$ ) and the distance between  $1\sigma$  errors bands ( $B_{D1\sigma}$ ). Besides, in our analysis we use statistics tools such as  $P$ -value, the Bayesian information criterion (BIC), the Akaike information criterion (AIC) and minimization of the  $\chi^2$  in order to perform a model selection according to the best values. In particular we work with two groups of models. The first group is aimed to contrast Core and Cusp models (Piso, NFW, Spano and Burkert) and the second one is aimed to compare Core, Cuspy, and Fuzzy models (Schive, NFW, and two hybrid Schive-NFW). Our criteria for model selection are: the best BIC value; the lowest  $B_{DIST}$  value and the lowest  $B_{D1\sigma}$  value. Additionally, from the statistical tools mentioned above and from the non-parametric reconstruction, a possible classification of galaxies as core or cuspy is investigated.

Finally, the scaling relationship of the DM haloes and the luminosity of the galaxies using a bayesian Markov Chain-Monte Carlo (MCMC) method are analyzed. In particular we study the characteristic volume density  $\rho_s$ , the scale length  $r_s$ , the characteristic central surface density  $\rho_s r_s$  and the central DM halo mass within 300 pc. We show that the scaling relations help us to understand better the core-cusp problem.

The structure of this work is as follows: in Sec. 2 we review the main properties of the galaxy rotation curves and the selection criteria of galaxies from SPARC we have worked with; in Sec. 3 we briefly summarize the LOESS and SIMEX techniques; in Sec. 4, we present the statistical methodology to perform the model selection; in Sec. 5 we report the results; in Sec. 6 the results are discussed and finally we end up with the conclusions in Sec. 7.

## 2 GALAXY ROTATION CURVES

Let us start by pointing out that we shall consider rotation curves of galaxies within the weak gravitational field limit in order to investigate DM parameters.

The rotation curve  $V(r)$  is obtained from the absolute value of the effective gravitational force as:

$$\begin{aligned} V^2(r) &= r \left| \frac{d\Phi(r)}{dr} \right| \\ &= \sqrt{G \frac{M_{DM}(r)}{r} + \Upsilon_{Disk} V_{Disk}^2 + V_{Gas}^2}, \end{aligned} \quad (1)$$

where  $\Phi(r)$  is the gravitational potential,  $M_{DM}(r)$  is the halo mass of the DM distribution,  $V_{Disk}$  and  $V_{Gas}$  are the contributions of the stellar disk and gas disk velocities and  $\Upsilon_{Disk}$  is the stellar mass-to-light ratio of disk. In  $V_{Gas}$  is already included the mass-to-light ratio  $\Upsilon_{Gas}$ .

The models we select to fit each rotation curve can be reviewed in the appendix A; there the explicit form of the density profile and the velocity function are included for

each case considered in this work. Specifically PISO, NFW, Spano, Burkert and the scalar field DM (SFDM) models.

Here we discuss only the less known SFDM cases (for a recent review see Bernal et al. (2018)). As was pointed out in the Introduction, large scale numerical simulations have provided two profiles. The first one is the NFW using CDM model, and, the second one, using SFDM, an inner soliton-like profile, that we called Schive Wave DM model (WDM), with an asymptotic NFW decline in the outer points, called Schive Wave+NFW DM (SNFW), Schive et al. (2014). At cosmological scales these two models are equivalent. However, CDM presents some challenges at the galactic level that can be solved using the Wave DM model because of its core nature. Moreover, Schive et al. (2014) derived an empirical density profile that described DM haloes with a soliton-like core embedded in an NFW density profile dominant at large radii. Such profile can be approximated by

$$\begin{aligned} \rho_{\text{SNFW}}(r) &= \Theta(r_\epsilon - r)\rho_{\text{WDM}}(r) \\ &+ \Theta(r - r_\epsilon)\rho_{\text{NFW}}(r), \end{aligned} \quad (2)$$

where  $\Theta$  is the step function,  $r_\epsilon$  the transition radius where density changes from the Schive profile

$$\rho_{\text{WDM}}(r) = \frac{\rho_w}{(1 + a_w(r/r_w)^2)^8}, \quad (3)$$

to the NFW profile Eq. (A6). Here  $a_w = 0.091$ ,  $\rho_w$  is the core density and  $r_w$  is its scale radius. Once  $\rho_w$  and  $r_w$  are fitted, the boson mass  $m_w$  is found using  $\rho_w = 1.9(m_w/10^{-23} \text{ eV})^{-2}(r_w/\text{kpc})^{-4} M_\odot \text{pc}^{-3}$ . The total density (2) has five parameters ( $\rho_w$ ,  $r_w$ ,  $r_\epsilon$ ,  $\rho_n$ ,  $r_n$ ), the last two parameters are defined in Eq. (A6). The last issue is related to the matching conditions at the transition radius  $r_\epsilon$  in Eq. (2). There are two possibilities. Either use only the continuity in the density function, or apply a continuity condition to the density function and its derivative. The former case yields four parameters to fit, while the latter case leaves us with three parameters to fit. The last SFDM model to consider is where the core part dominates the galaxy. In such a case Eq. (2) reduces to only the first term,  $\rho_{\text{WDM}}(r)$ , with two parameters to fit. The complete expressions for all models are given in the Appendix A.

Regarding the galaxy selection, we are considering the baryonic contribution for each rotation curve of SPARC (Disk and Gas), the same values of  $\Upsilon_{\text{Disk}} = 0.5 M_\odot/L_\odot$  at  $3.6 \mu\text{m}$  and  $\Upsilon_{\text{Gas}} = 1.33 M_\odot/L_\odot$  (Schombert & McGaugh 2014; Lelli et al. 2016; Lelli et al. 2017).

Since for the fitting we shall assume a considerable contribution of dark matter, we choose galaxies from the SPARC catalogue (Lelli et al. 2016) for which the percentage of dark matter contribution lies between  $90 > f_{\text{DM}} > 60$ , where  $f_{\text{DM}}/100 = M_{\text{DM}}(r_{\text{max}})/(M_{\text{Bar}}(r_{\text{max}}) + M_{\text{DM}}(r_{\text{max}}))$ ,  $M_{\text{DM}}$  corresponds to the dark matter contribution for each model, and  $M_{\text{Bar}}$  is the total baryonic mass, both evaluated at the outer value of the observed radius of the rotation curve  $r_{\text{max}}$ .

Within our sample, we classify galaxies according to the dominant baryonic component, consequently, those dominated by gas are of the order of 83.3%, the ones dominated by the stellar disk, 14.6% and 2.08% where the gas and the stellar disk contribute with the 50% from the total photometric information (NGC 0300, for example). However, according to the morphology of the galaxies and the Hubble classification, we have a galaxy selection where  $\sim 33.3\%$  are

Sm, 27.08% Im, 20.83% Sd, Scd = Sdm = 6.25%, 4.17% Sc and 2.08% BCD (Lelli et al. 2016).

In the following section we briefly review the non-parametric curve fitting method employed in our sample.

### 3 NON-PARAMETRIC RECONSTRUCTION METHOD

#### 3.1 Basis of LOESS

LOESS is a non-parametric method in the sense that the fitting is performed without having to specify in advance the relationship between the dependent and independent variables. At each point of the data set a low-degree polynomial is fit to a subset of this data, the polynomial is obtained by weighted least squares, giving more weight to points near to the point whose response is being estimated and less weight to points further away. The value of the regression function for the point is then obtained by evaluating the local polynomial using the independent variable value for that data point. The LOESS fit is complete after regression function values have been computed for each of the  $n$  observational measurements. This whole process offers the possibility to get the full view of the global trend of the data, which is the original objective of the procedure. To obtain the graphical account of the relationship between dependent and independent variables, it suffices to join the reconstructed points with a line.

Here we work with observational data of rotation curves of galaxies, so the radius  $R$ , measured in kpc, will be our independent variable while the velocity  $V$  of the stars or gas particles, in units of km/s, corresponds to the dependent variable.

In the following the main elements of the method are briefly discussed. For further details we encourage the reader to see Montiel et al. (2014) and references therein.

##### i. Smoothing Parameter

The *smoothing parameter*,  $s$ , also called *span* determines how many data points should be used in each weighted least squares fit. The *span* ranges between 0 and 1 and controls the flexibility of the LOESS regression function. Large values of  $s$  produce the smoothest functions that wiggle the least in response to fluctuations in the data but small values of  $s$  produce more irregular reconstructed curves, because the intrinsic noise and dispersion of data is fully captured. Choice of the span, the degree of polynomial, and the weight function can all affect the trade-off between the bias and variance of the fitted curve, however, the value of the span has the most important effect as can be seen in Fig. 1, in which the differences in the fitted regression curves are associated to the choice of span. In order to minimize this effect, as in Montiel et al. (2014), the election of the optimal value of the *span*  $s$  is done by using the *cross-validation* method which aims to minimize the mean squared error of the fit.

##### ii. Weight Function

As mentioned above, the weight function assigns a large weight to the data points nearest the point of estimation and a low weight to the data points that are furthest away. The usual weight function employed for LOESS is the tri-

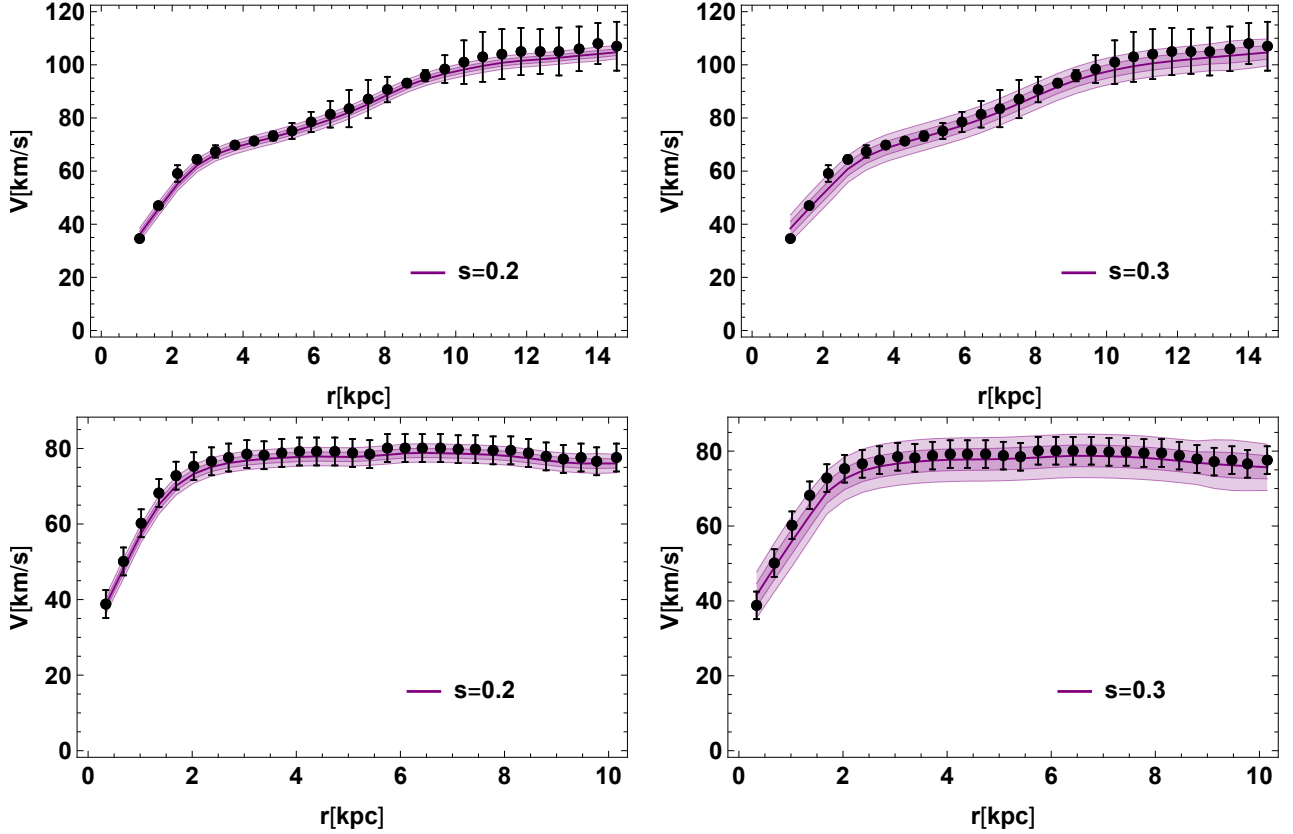


**Figure 1.** LOESS reconstruction for the NGC0247 (upper figures) and UGC08490 (lower figures) galaxies, obtained by using different values for the span,  $s$ , showing the impact of the choices of  $s$  in the reconstructed curve (regardless the observational errors).

cube weight function,

$$w(x) = \begin{cases} (1 - |x|)^3 & \text{for } |x| < 1 \\ 0 & \text{for } |x| \geq 1 \end{cases} \quad (4)$$

However, any other weight function that satisfies the properties listed in [Cleveland \(1979\)](#) is also useful. Such properties are a positive weight function and even a treatment of points left and right of each point  $x_i$ . In addition, it is desirable that  $w(x)$  decreases smoothly to 0 as  $x$  goes from 0 to 1. Among the weight functions that decrease to 0, normally the tricube function is chosen since it provides an adequate smoothing in almost all cases. Here, as in [Montiel et al. \(2014\)](#), this weight function is used.

### iii. Degree of Local Polynomials

The idea behind LOESS is to fit each subset of data using polynomials of a low degree after the weight function is applied. Most of the polynomials are of first or second degree and although higher-degree polynomials would work, it could cause overfit of the data in each subset, besides of higher computational cost without any significant improvement in the result.

### iv. Confidence regions

In order to construct the confidence regions of the nonparametric regression we perform an analogy with the standard least squares regression by using the local polynomial estimate,  $\hat{y}_i$ , that results from the locally weighted least-squares

regression of  $y$  on the  $x$  values in each chosen window  $i$ . Thus, by assuming normally distributed errors, the 68%-percent confidence interval and the 95%-percent confidence interval of the regression function can be constructed.

It is worth mentioning that this procedure for constructing a confidence region is not completely accurate, due to the bias in  $\hat{y}_i$  as an estimate of the regression function [Fox \(2000\)](#). The value of the smoothing parameter changes significantly the function estimate, and consequently the confidence bands. In this sense, such a bias can produce an overestimation of the error variance, thus making the confidence interval too wide. On the contrary, an inadequate small span (i.e. with insufficient data within the window fit) yields large variance. As we have pointed out, this can be alleviated by using the cross-validation procedure in order to choose the optimal value of  $s$  as is suggested in [Montiel et al. \(2014\)](#).

## 3.2 Basis of SIMEX

SIMEX method is based on two resampling approaches. At the first stage, the simulation, additional errors are introduced in the data by using a controlling parameter  $\lambda$ . Next, a regression analysis is used on this new dataset to trace the effect of the measured error in the original dataset [Cook & Stefanski \(1994\)](#); [Stefanski & Cook \(1995\)](#). More specifically, SIMEX work as follows:

- 1.- The *simulation step*. The method starts by introducing



additional errors on each observation  $y_i$  in the data set, with  $i = 1, \dots, n$  and  $n$  the number of data points, following the rule

$$\eta_i(\lambda) = y_i + \sqrt{\lambda}\sigma_i, \quad \lambda > 0 \quad (5)$$

where  $\sigma_i$  is the measurement error variance associated to the observed data  $y_i$  and the parameter  $\lambda$  acts as the controlling parameter for the amount added of  $\sigma_i$ . We take, as in Montiel et al. (2014),  $\lambda = \{0.5, 0.6, 0.7, \dots, 2.0\}$  to simulate the *new* datasets.

**2.- The extrapolation step.** After introducing the variable  $\lambda$ , the final measurement error variance associated with the simulated data points,  $\eta_i(\lambda)$ , is  $(1 + \lambda)\sigma_i^2$ . So, it is necessary to take  $\lambda \rightarrow -1$ , in order to return back to the original data without uncertainties and to trace the effect of the measured error in the original data. This is done via a regression analysis, using a quadratic polynomial, on the *new* datasets.

Up to this point, we have addressed briefly the features and free parameters of the *LOESS+SIMEX* method, however many more details can be found in Fox (2000); Andersen (2009); Han (2012); Shalizi (2012); Wasserman (2006); Carroll et al. (1995); Cook & Stefanski (1994); Stefanski & Cook (1995); Carroll et al. (1999); Montiel et al. (2014) and references therein.

#### 4 PARAMETRIC AND NON-PARAMETRIC STATISTICAL METHODOLOGY

We have selected 88 galaxies from SPARC with an important contribution of DM to the rotation curve in order to study, from the non-parametric and parametric point of views, the seven theoretical models that we have pointed out before. This section reviews how we perform the estimation of the best fit parameters as well as the statistical tools used to perform the model selection.

Regarding the parametric approach, which focuses on estimating the model parameters, we use a fitting code to minimize the reduced  $\chi_{red}^2$  function,

$$\chi_{red}^2 = \frac{1}{N_d - N_p} \sum_{i=1}^N \frac{(V_{obs}(r_i) - V_{model}(r_i, \hat{\theta}))^2}{\delta V_{obs}^2(r_i)}, \quad (6)$$

where  $V_{obs}$  and  $\delta V_{obs}$  are the observed galaxy velocity rotation curve and its uncertainty at the observed radial distance  $r_i$ ,  $\hat{\theta}$  are the  $N_p$  fitting parameters of every model studied and  $N_d$  is the total number of data. Remember that  $\chi_{red}^2 \sim 1$  is desirable for a good fit (Press et al. 2007).

We also compute the  $P$ -value ( $\chi^2$  test) which is an indicator between the compatibility of the distribution data and the fitting model.  $P > 0.95$  indicates that we have a ( $> 95\%$ ) chance of finding a result less close to the central data; while if  $P < 0.05$ , the data and the fitting model are incompatible and then we can reject the fitting model; in case that  $P > 0.05$  we can not reject the model (Press et al. 2007).

Since we are comparing models with a different number of parameters, we compute the AIC (Akaike information criterion) and the BIC (Bayesian information criterion) in order to perform the model selection. In these statistical

methods there is a penalty, which is applied to compensate for the obligatory difference in likelihoods due to the different number of parameters (Feigelson & Babu 2012). That is, if we have a model  $M_j$  with a  $p_j$  parameters  $\hat{\theta}_j$ , then

$$AIC = -2l(\hat{\theta}_j) + 2p_j, \quad (7)$$

where  $2l(\hat{\theta}_j)$  is the goodness-of-fit term and  $2p_j$  is the penalty of number of parameters. On the other hand, the Bayesian information criterion is defined as

$$BIC = -2l(\hat{\theta}_j) + 2p_j \ln N_d, \quad (8)$$

where, as before,  $N_d$  is the number of data points.

The goodness-of-fit definition used in both cases is

$$l(\hat{\theta}_j) = \prod_i \frac{1}{\sqrt{2\pi\delta V_{obs}^2(r_i)}} \exp\left(-\chi_j^2\right), \quad (9)$$

where  $\chi_j^2$  and  $\delta V_{obs}^2(r_i)$  describe the galaxy studied, Eq. (6), and are associated to the  $j$ -model (Cousineau & Allan 2015).

AIC penalizes free parameters less strongly than does the BIC. BIC imposes a greater penalty for larger datasets while the AIC is independent of the sample size.

The galaxies we have analyzed are the ones that fulfill the quality condition (see McGaugh et al. (2016)). We used a Markov Chain-Monte Carlo (MCMC) method (Gamerman 1997) implemented in *Mathematica* by one of the authors (MARM),<sup>1</sup> in order to constrain the free parameters of the DM models through a maximization of the likelihood function  $\mathcal{L}(\mathbf{p})$  given by

$$\mathcal{L}(\hat{\theta}_j) = \frac{1}{(2\pi)^{N_d/2} |\mathbf{C}|^{1/2}} \exp\left(-\frac{\Delta^T \mathbf{C}^{-1} \Delta}{2}\right), \quad (10)$$

where  $\hat{\theta}_j$  is the vector of parameters,  $\Delta = V_{obs}(r_i) - V_{model}(r_i, \hat{\theta}_j)$  and  $V_{model}$  the derived total velocity for one of the seven models computed in the same position where  $V_{obs}$  was measured, and  $\mathbf{C}$  is a diagonal matrix.

We sample, using the Metropolis Hastings algorithm, the parameter space from uniform prior ranges with two Markov chains and tested the convergence of the fit with the Gelman-Rubin convergence criterion ( $\mathcal{R} - 1 < 0.01$ ) (Gelman & Rubin 1992). The fitting parameters and the 1  $\sigma$  and 2  $\sigma$  confidence levels (CL) are computed from the Markov chains with 30% of burn-in. We have tested the MCMC code against the results obtained with the minimization method described above. The Markov chain was analyzed using Get-Dist code that is included in the CosmoMC code (Lewis & Bridle 2002).

On the other side, regarding the nonparametric approach, we would like to recall we are using a technique which focuses on the fitted curve such that the fitted points and their errors are estimated with respect to the whole curve rather than a particular estimate and then, the overall uncertainty is measured on the basis of how well the estimated curve fits the data.

Since LOESS+SIMEX reconstruction has been used in an informal graphical way to assess the relationship between variables in Montiel et al. (2014); Rani et al. (2015);

<sup>1</sup> Public at <https://github.com/rodriguezmeza/MathematicaMCMC-1.0.0>

Escamilla-Rivera & Fabris (2016); Rana et al. (2016), in order to check the validity of a specific theoretical model by comparing with the nonparametric regression curve, we compute the distance between the best  $\chi^2$  fitted velocity curve and the velocity curve obtained by reconstruction and also the distance between the  $1\sigma$  band from the best  $\chi^2$  fitted curve and the  $1\sigma$  band from LOESS+SIMEX one.

We define the distance (area) between curves as:

$$D = \frac{\int_{r_{min}}^{r_{max}} |V_{\text{LOESS}}(r) - V_{\text{model}}(r, \hat{\theta})| dr}{A_{\text{DATA}}}, \quad (11)$$

where  $V_{\text{LOESS}}(r)$  is the reconstruction velocity rotation curve from the data distribution,  $V_{\text{model}}(r, \hat{\theta})$  is the velocity function of each model characterized with their parameters  $\hat{\theta}$ . Notice we are normalizing the area between curves with  $A_{\text{DATA}}$ , which is the area enclosing the velocity rotation data, including the error bars.

For the distance (area) between  $1\sigma$  bands (model and LOESS+SIMEX) we take into account the following cases:

- If there is not overlap between bands at a given  $R$  and the LOESS  $1\sigma$  band is above the model  $1\sigma$  band, there we compute its contribution to the distance as

$$\delta D = \frac{1}{A_{\text{DATA}}} \int_R^{R+\delta R} |V_{\text{LOESS}}^L(r) - V_{\text{model}}^U(r, \hat{\theta})| dr, \quad (12)$$

where  $V_{\text{LOESS}}^L(r)$  is the lower curve of the LOESS  $1\sigma$  band and  $V_{\text{model}}^U(r, \hat{\theta})$  is the upper curve of the model  $1\sigma$  band. When the model  $1\sigma$  band is above the LOESS  $1\sigma$  band, we use a similar expression.

- If there is an overlap between the  $1\sigma$  bands but one band is inside the other there  $\delta D = 0$ . On the opposite case, if  $V_{\text{LOESS}}^U(r) > V_{\text{model}}^U(r, \hat{\theta})$  the contribution to the distance is given by

$$\delta D = \frac{1}{A_{\text{DATA}}} \int_R^{R+\delta R} |V_{\text{model}}^U(r, \hat{\theta}) - V_{\text{LOESS}}^U(r)| dr. \quad (13)$$

If  $V_{\text{model}}^U(r, \hat{\theta}) > V_{\text{LOESS}}^U(r)$  the contribution to the distance is given by a similar expression.

## 5 RESULTS

In Table B1 we show the statistical results for PISO (1), NFW (2), Spano (3) and Burkert (4) models and for the galaxy selection of the SPARC catalog where DM is dominant.

For each model we report the  $\chi_{red}^2$ ,  $P$ -value, AIC, BIC, distance between the best fit velocity curve and the reconstruction with LOESS+SIMEX (DIST), the distance between the  $1\sigma$  band from the best fit and the  $1\sigma$  band from LOESS+SIMEX ( $D_{1\sigma}$ ). Also in columns 26–29, the Best Model columns are shown according to the BIC value ( $B_{\text{BIC}}$ ), the distance between the LOESS+SIMEX reconstruction and the best fit curves ( $B_{\text{DIST}}$ ), the distance between  $1\sigma$  bands  $B_{D_{1\sigma}}$  and  $\chi_{red}^2$  value. Columns 26–28 with models ordered according to the best values allow us to establish the three conditions as a criterion to accept or reject models. The ordering is as follows.

In the table we associate a number (1–4) to each model,

and for column 26 and according to the best BIC (the model with the minimum value in the BIC), we write in the first place the number of the model to point out the best one. Followed by the second one that has the best BIC among the rest, and so on. We found from the comparison of the best BIC's that the success for PISO is  $\sim 15.9\%$ , for NFW  $\sim 18.1\%$ , Spano  $\sim 46.6\%$  and for Burkert  $\sim 18.2\%$ .

In columns 27 and 28 of Table B1 we show, in ascending order, the models (1–4) according to the distance between LOESS+SIMEX and best fit velocity curve ( $B_{\text{DIST}}$ ) and the distance between the  $1\sigma$  confidence bands for LOESS+SIMEX and best fit velocity rotation curve, ( $B_{D_{1\sigma}}$ ), respectively.

From this table and according to the lower BIC, the lower distance  $B_{\text{DIST}}$  and lower distance  $B_{D_{1\sigma}}$ , the percentage of galaxies satisfying the three conditions, i. e., galaxies that have the best values in all the cases, is the 44.32%. From this 44.32% of the analyzed galaxies, approximately the 53.85% points out to Spano as the most favored model and for NFW  $\sim 20.51\%$ , for PISO we found a percentage value of  $\sim 10.25\%$  and Burkert  $\sim 12.82\%$ .

It is important to mention that BIC and AIC have the same penalty term, therefore the best AIC is compatible 100% with the best BIC value.

Finally, as an additional information, we show in column 29 the best  $\chi_{red}^2$ , in this case the first number indicates the model with the lower  $\chi_{red}^2$ . It is important to mention that, in this group, the number of parameters of each model is the same, therefore there is a consistency between AIC and BIC definitions where the selection of the most favorable model according to the AIC has a coincidence of 100% with the selection of the best BIC (in this case the model order for each galaxy according to AIC is the same according to BIC).

As a way to illustrate the considerable differences between the models studied in this work, by taking a look to the Best Model columns of Table B1 (columns 26–28), we choose four galaxies where the distance between the fitting velocity curve and the nonparametric reconstructed curve (central lines and  $1\sigma$  bands) is the biggest for the NFW model. Also in agreement with the respective BIC results and  $\chi_{red}^2$ , the four columns of the Best Model select NFW in the last place.

In Figs. 2 and 3 we show the observed rotation curves for four galaxies and the rotation curves that result from the fitting procedure with four models, PISO, NFW, Spano and Burkert. In these figures are shown the curves resulting from the nonparametric LOESS-SIMEX procedure (in cyan). The red colors are for the best fit curves,  $1\sigma$  and  $2\sigma$  error bands, respectively. For the galaxies DDO 154, IC 2574, NGC 3109 and UGC00891 (Fig. 2), and for NFW model the distance between the best fit and  $1\sigma$  bands has a noticeable separation from the LOESS-SIMEX band and in agreement with results shown in Table B1. And in Fig. 3 we show that for the rotation curves NGC 0024, NGC 0247, NGC 3741 and UGC 05716, Spano and Burkert models are having the biggest distance between the  $1\sigma$  confidence and the reconstruction LOESS+SIMEX confidence bands, even the columns of the Best Model place Spano in the last place of the selection.

On the other hand, keep in mind that LOESS+SIMEX can provide great assistance in model selection, particularly when the data are very noisy or have other features that

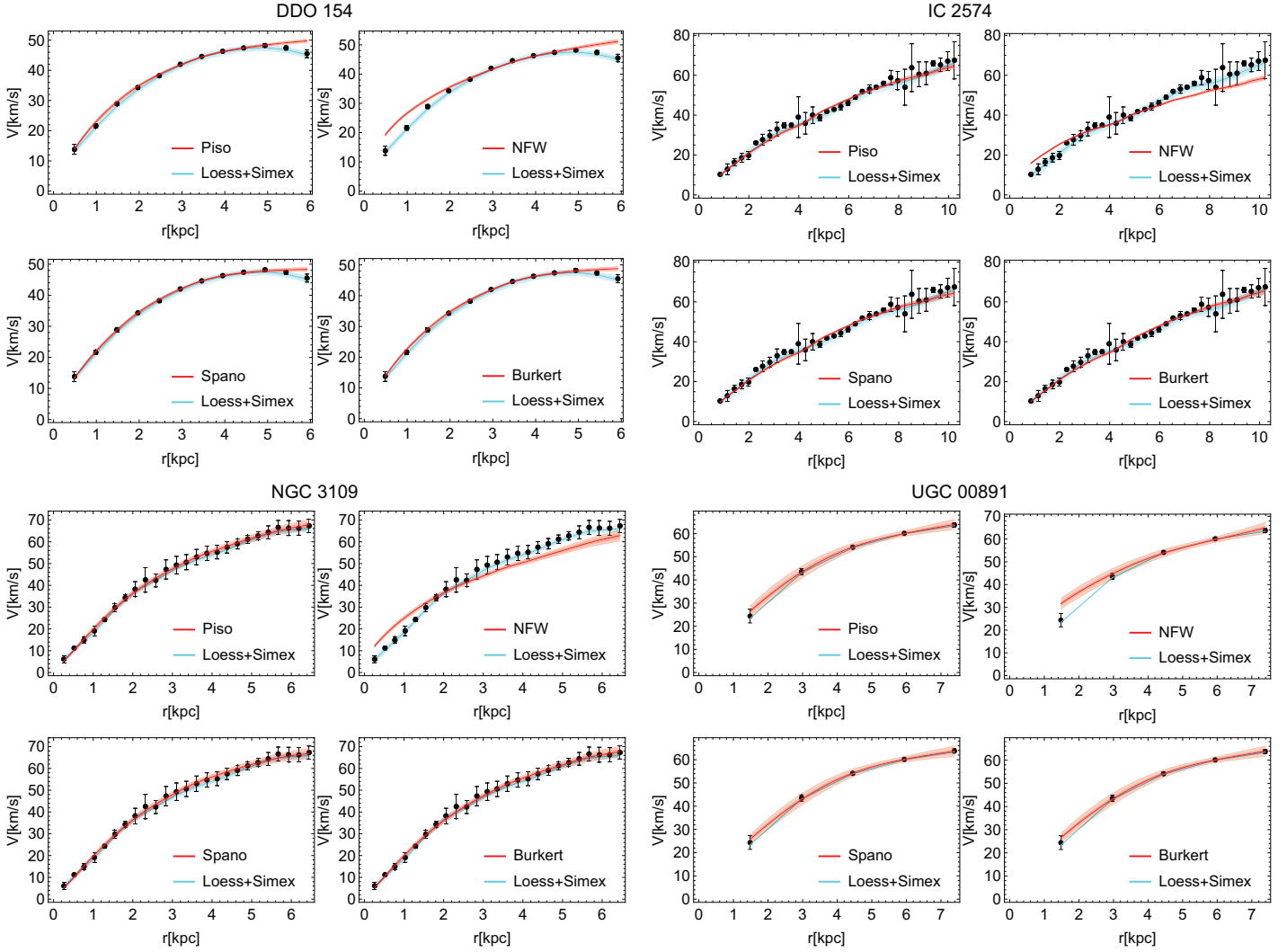


**Figure 2.** Galaxies where the distance between the best fit and  $1\sigma$  bands for NFW has a notable separation with the LOESS+SIMEX band, according with the results from Table B1. In the figure we show the reconstruction LOESS+SIMEX  $1$  and  $2\sigma$  bands in cyan color, the best fit for the four studied models in the second group including  $1$  and  $2\sigma$  bands in red.

make patterns difficult to see. Indeed, following Azzalini et al. (1989), a very simple way to assess the goodness of fit of a parametric model is by determining if the nonparametric fit falls within the parametric error bars. So, if we take a look at Fig. 2 and the respective plots for the NFW model, for all the galaxies showed there, it is noticeable that the reconstructed curve lies outside the error bands of NFW model which indicates that this model does not appear to be a good fit to these data which gives support to our results that point out NFW is not the most favored model. The same argument can apply to other figures.

Taking as reference the NFW model, we studied the Schive and the Fuzzy models (SNFWDC and SNFWC) to compare the quantitative distances between the best fitting and the LOESS+SIMEX method. From this group of models we compare core, cusp and fuzzy models, where in addition, these fuzzy models have the freedom to adapt themselves to the structure of each galaxy and reproduce either core or cusp models. The value of  $r_\epsilon$ , Eq. (A14), can provide us

the three different structures of a galaxy: Core ( $r_\epsilon > r_{\max}$ , being  $r_{\max}$  the last observed radius of the galaxy), Cusp ( $r_\epsilon \sim r_{\min}$  with  $r_{\min}$  is the first observed radius of the galaxy) and Core+Cusp ( $r_{\min} < r_\epsilon < r_{\max}$ ).

The results of the analysis of this group of models are shown in Table B2. Its description is similar to Table B1. Columns 27–30 show the Best Model values, from 27–29 we apply our selection criteria. In order to obtain an alternative classification value for the baryonic contribution in each galaxy, we compute  $\delta A_V = 100 \frac{A_{V\text{Bar}}}{A_{V\text{Obs}}}$ , where  $A_{V\text{Bar}}$  is the total area enclosed by the baryonic velocity contribution,  $\sqrt{\Upsilon_{\text{Disk}} V_{\text{Disk}}^2 + V_{\text{Gas}}^2}$  and  $A_{V\text{Obs}}$  is the area under the velocity rotation curve of the observed data (in the radius range observed), see column 2 of Table B2.

Here, it is important to mention that we have three galaxies where the number of observed data is the same as the number of free parameters for the SNFWC model (we use the \* symbol, next to the galaxy name to identify these galaxies, see Table B2); in these cases we are not report-

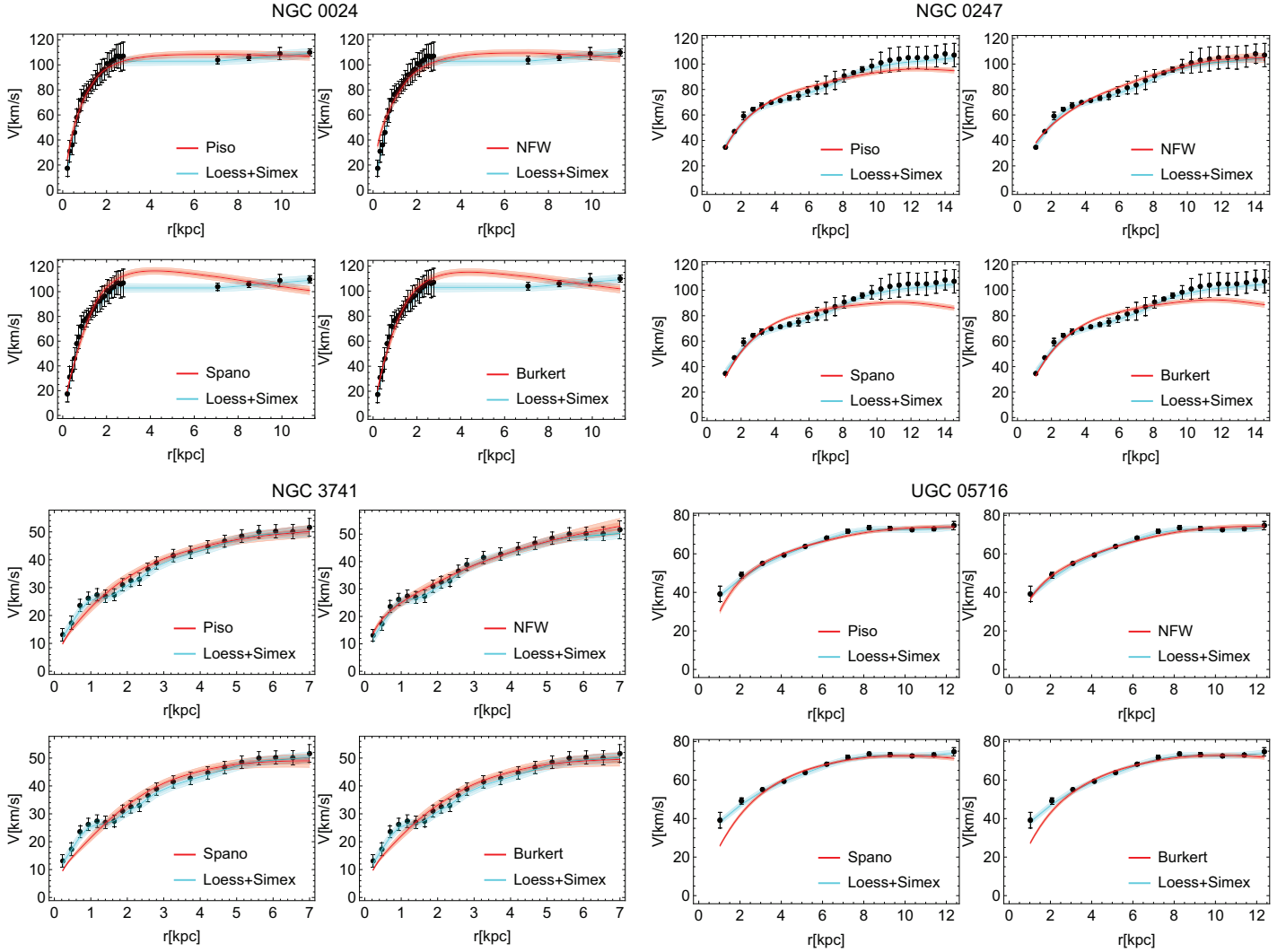


**Figure 3.** Galaxies where the distance between the best fit and  $1\sigma$  bands for Spano and Burkert have a notable separation with the LOESS+SIMEX band, according with the results from Table B1. In the figure we show the reconstruction LOESS+SIMEX 1 and  $2\sigma$  bands in cyan color, the best fit for the four models studied in the second group including 1 and  $2\sigma$  bands in red.

ing the  $\chi^2_{red}$  and the  $P$ -value, nevertheless it is possible to calculate the other statistic quantities.

In Figs. 4 and 5 we show the observed rotation curves for four galaxies and the rotation curves that result from the fitting procedure with the four models, NFW, Schive and the Fuzzy models. The resulting curves from the nonparametric LOESS-SIMEX procedure are displayed as well. The cyan bands are the nonparametric reconstruction LOESS+SIMEX and the red colors are for the best fit curves,  $1\sigma$  and  $2\sigma$  error bands, respectively.

From Table B2 we studied the relationship between the lower BIC and the lower value from  $B_{DIST}$  and  $B_{D1\sigma}$ , and we found that  $\sim 28.41\%$  of galaxies satisfy the three conditions. In this case Schive has been selected with the 44% to be the most favored model, NFW with 36%, SNFWDC 12% and SNFWC obtained 8% of model selection coincidence.

It is important to mention that even when BIC and AIC have different penalty terms, the best AIC is compatible  $\sim 76.1\%$  with the best BIC value, which gives us a strong

support for the Best Selection Model techniques used in this work.

According to the Best Model columns from Table B2, we notice that the  $B_{DIST}$  selection model is the same for the Fuzzy models (3 and 4) in 24 galaxies, and 11 galaxies where fuzzy models have the same  $B_{D1\sigma}$ . If we considered the cases where  $B_{DIST}$  and  $B_{D1\sigma}$  have the same value for the Fuzzy models (3 and 4) we found that only 8 galaxies fulfill this condition. For example, let us consider the galaxy NGC 0247 and compare the two columns  $B_{DIST}$  and  $B_{D1\sigma}$  (from the Best Model column) and we found the combination (34) in first and second place of the numerical combination of models, respectively. This is because  $r_{\epsilon}^{(3)} \sim r_{min}$  and  $r_{\epsilon}^{(4)} < r_{min}$ , which tell us that NFW model fits better the structure for the rotation curve. For the other cases, galaxies DDO 064, DDO 168, KK 98-251 we obtain  $r_{\epsilon}^{(3)} > r_{max}$  and  $r_{\epsilon}^{(4)} > r_{max}$ , where Schive is the dominant model for the rotation curves; for UGC 05716, UGC 07399 and UGC 08490  $r_{\epsilon}^{(3)} <$



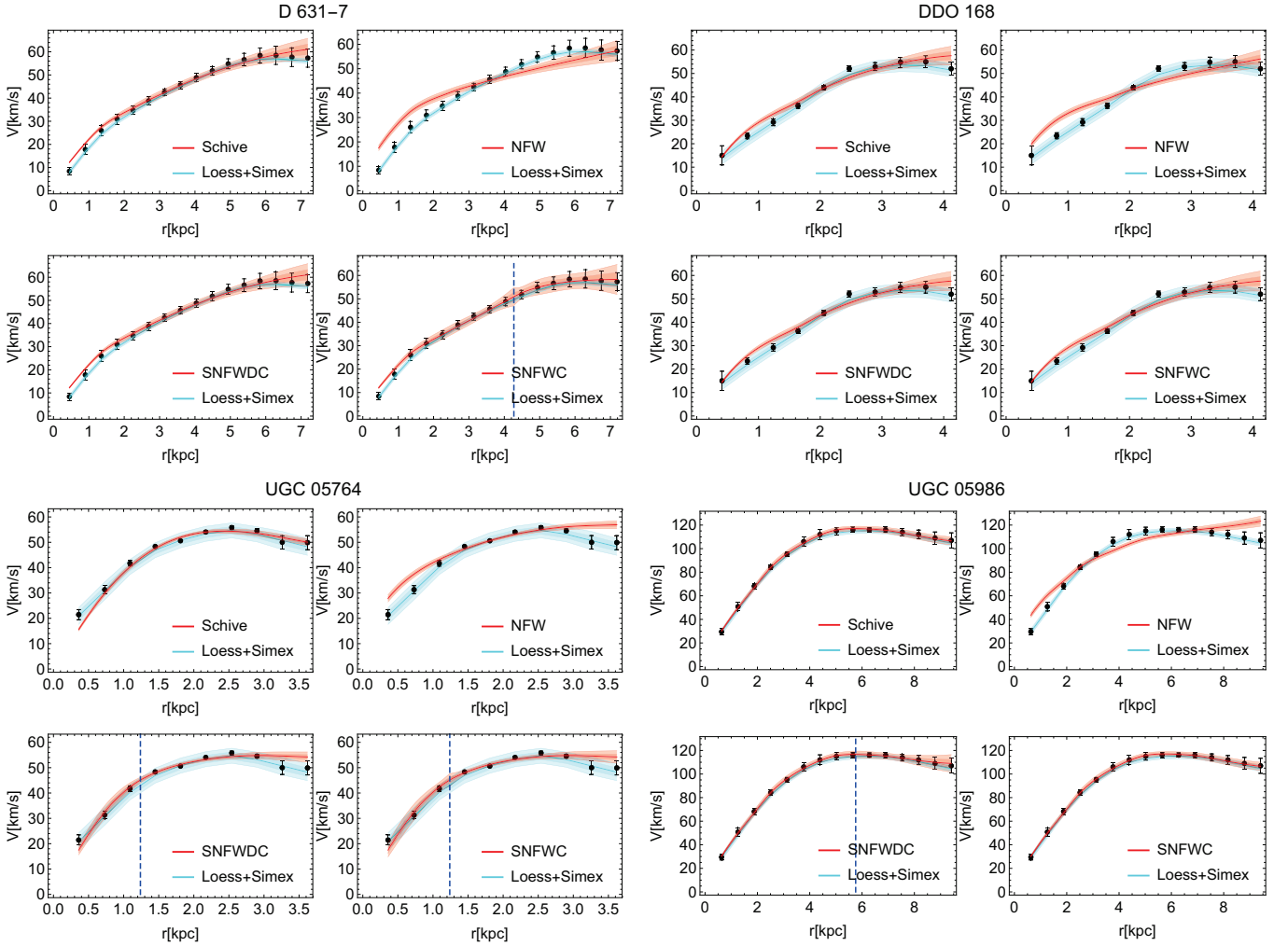


**Figure 4.** Galaxies where the distance between the best fit and  $1\sigma$  bands for NFW has a notable separation with the LOESS+SIMEX band, according with the results from Table B2. In the figure we show the reconstruction LOESS+SIMEX 1 and  $2\sigma$  bands in cyan color, the best fit for the four models studied in the second group including 1 and  $2\sigma$  bands in red and the vertical lines correspond to  $r_\epsilon$  (transition radius for the fuzzy models, Eq. (A14)).

$r_{min}$  and  $r_\epsilon^{(4)} < r_{min}$ ; and for UGC 07524  $r_\epsilon^{(3)} = r_\epsilon^{(4)} = 3.378$  kpc.

Additionally, we notice that Schive model has problems in fitting the data points while NFW in the initial data. On the other hand, Fuzzy models solve the two problems, the transition radius  $r_\epsilon$  for each SNFW model is the same for 13 galaxies, while, for the other 35 galaxies we have for SNFWDC (3),  $0.11 < r_\epsilon^{(3)} < 9.4$  and for SNFWC (4),  $0.15 < r_\epsilon^{(4)} < 19.7$ . In the cases where SNFW models are the same, we use the  $B_{BIC}$  in order to perform the model selection because it considers the penalty term for the number of parameters instead of taking the  $B_{D1\sigma}$  which can lead to misleading results due to the error propagation in the LOESS+SIMEX technique.

So far we have compared the results obtained from parametric versus non-parametric analysis. The SPARC subsample consists of 88 rotation curves of galaxies with quality factor  $Q = 1$  or 2. To find any indication of spatial resolution effect on the results we have divided the subsample into two: the first one with only galaxies with a  $Q$  value of 1 (50

galaxies) and the second one with  $Q = 2$  (38 galaxies). The analysis results are as follows:

**Q= 1** When the RC is extracted from the first group Table B1: we found that 36% satisfied the three conditions and of which 55.56% prefer Spano model while 16.67% avored NFW. And for the RC extracted from the second group Table B2: 24% satisfied the three conditions and 33.33% support Schive as the best model according to the criteria and 25% favored NFW and 25% were also in favor of SNFWDC.

**Q= 2** If the RC is extracted from the second group Table B1: we found that 55.26% satisfied the three conditions and from them 52.38% favored Spano model and 23.81% favored NFW. Table B2: for  $Q = 2$ , 34.21% satisfied the three conditions and 53.85% of these favored Schive as the best model according to the criteria and 46.15% set to the NFW model in second place.

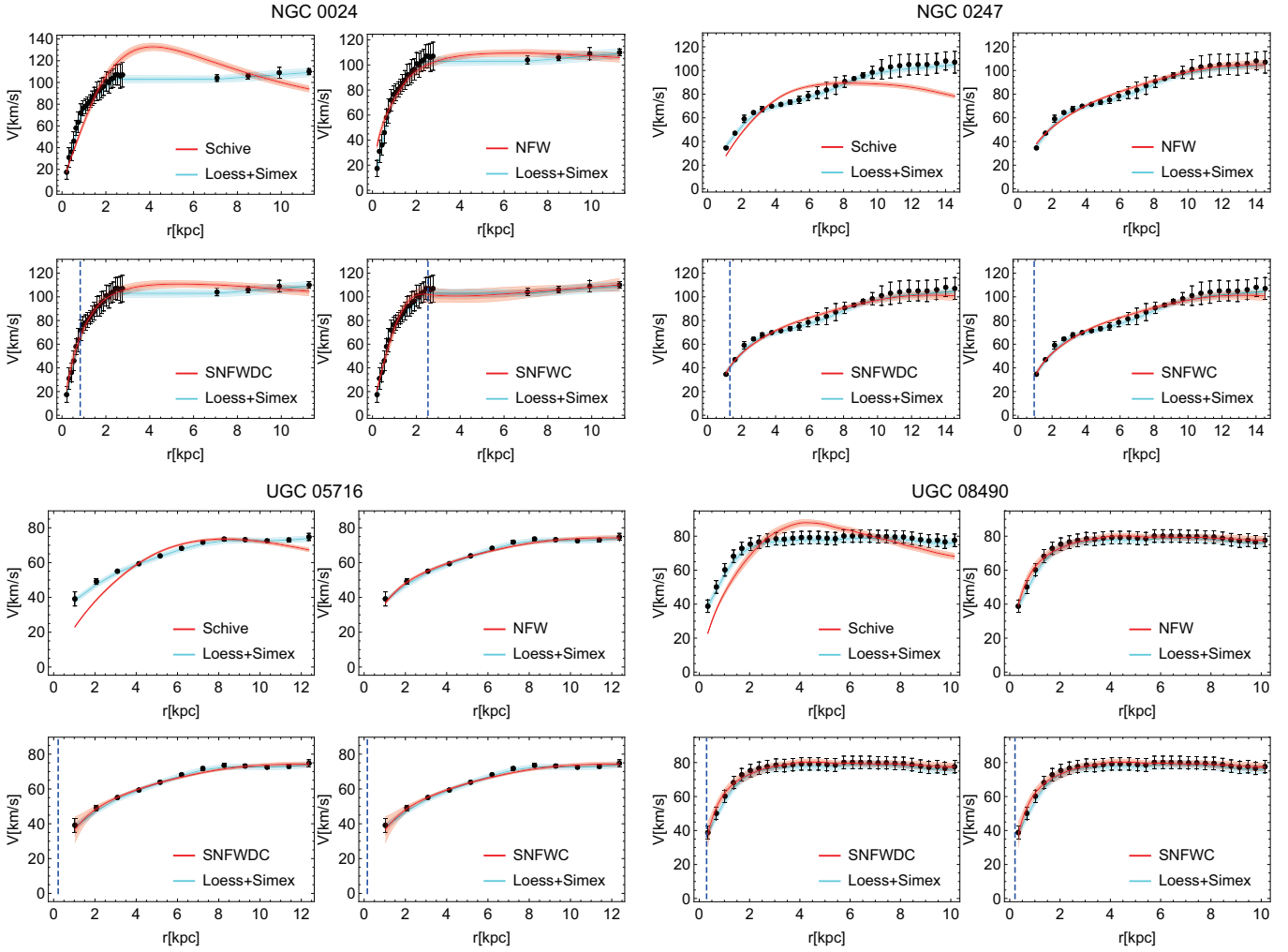


**Figure 5.** Galaxies where the distance between the best fit and  $1\sigma$  bands for Schive has a notable separation with the LOESS+SIMEX band, according with the results from Table B2. In the figure we show the reconstruction LOESS+SIMEX  $1$  and  $2\sigma$  bands in cyan color, the best fit for the four models studied in the second group including  $1$  and  $2\sigma$  bands in red and the vertical lines correspond to  $r_\epsilon$  (transition radius for the fuzzy models, Eq. (A14)).

## 6 DISCUSSION

From Table B2 and according to the three columns of the Best Model it is possible to classify the galaxies DDO 064, DDO 168, F 571-v1, KK 98-251, NGC 6789, UGC 05986 and UGC 06399 as core type, where this criterion points out to Schive as the best model.

In the same way we select the cuspy models based on Tables B1 and B2, observing that the Galaxies UGC 05716 and UGC 08490 point out to NFW (with the three conditions fulfilled in both cases) as the most favored model. On the other hand, UGC 02259, UGC 05918 and UGC 12732 are selected to be cuspy from Table B2, NGC 0247 and NGC 3741 from Table B1, satisfying again the three Best Model columns.

Comparing the two tables (seven models) for NGC 0247, NGC 3741, UGC 02259, UGC 05918 and UGC 12732 we found:

- For NGC 0247 comparing the seven models it is found that  $B_{\text{BIC}}$  and  $B_{\text{DIST}}$  point out to SNFWDC (3) and  $B_{\text{D1}\sigma}$

selects the NFW model. Analyzing the fuzzy models it is found that  $r_\epsilon^{(3)} = 1.31$  kpc and the minimum radius observed for this galaxy is  $r_{\text{min}} = 1.08$  kpc. In this case the major contribution in fitting the velocity of the galaxy comes from NFW ( $r_\epsilon^{(3)} \sim r_{\text{min}}$ , Fig. 5), therefore the fuzzy model is in agreement with LOESS+SIMEX and the other conditions to classify it as a cuspy galaxy.

- For NGC 3741, the NFW model satisfies  $B_{\text{BIC}}$  and  $B_{\text{D1}\sigma}$  and while the  $B_{\text{DIST}}$  points out to SNFWDC, but  $r_\epsilon^{(3)} = 0.268$  kpc and  $r_{\text{min}} = 0.23$  kpc which NFW gives the biggest contribution to the galaxy structure, as an additional condition, we compare the  $B_{\chi^2_{\text{red}}}$  for the seven models and found that this points out to NFW, therefore, we can classify NGC 3741 as a cuspy galaxy.

- For UGC 12732 we found that the NFW profile satisfies  $B_{\text{BIC}}$  and  $B_{\text{DIST}}$ , while PISO satisfies  $B_{\text{D1}\sigma}$  and the  $B_{\chi^2_{\text{red}}}$  points out to SNFWDC, where  $r_\epsilon^{(3)} = 0.8$  kpc and  $r_{\text{min}} = 0.96$  kpc. We can conclude that this galaxy is classified as a cuspy one.

The remaining galaxies (UGC 02259, UGC 05918) can be excluded of being cuspy because of NFW satisfies only  $B_{\text{DIST}}$  for both of them while PISO satisfies the rest of the conditions from Best Model column.

Additionally, in Fig. 4, we show four galaxies (D 631-7, DDO168, UGC 05764 and UGC 05986) with the four models (Schive, NFW, SNFWDC and SNFWC) from there, one can see that NFW is at a far distance from the confidence bands. From Table B2 we notice that these galaxies have in common that the NFW is in the last place from the selection number code of models. In contrast we observe in Fig. 5 (for galaxies, NGC 0024, NGC 0247, UGC 05716 and UGC 08490) that the Schive model best fit is far from the reconstruction. In these cases, Schive comes in the last place for the selection of the best model in Table B2.

To complement the comparison between non-parametric versus parametric methods of data analysis and in order to set some basic concepts to make an interpretation of our results, we have analyzed with the MCMC method the 152 galaxies that satisfy the quality condition of McGaugh et al. (2016) in the SPARC catalog of rotation curves.

For each halo DM model in the core-cusp group (see below) we have computed four important quantities that should give us information about galaxy formation and evolution: the central characteristic volume density  $\rho_s$ , the scale length  $r_s$ , the characteristic surface density  $\mu_{DM} \equiv \rho_s r_s$  and the DM mass within 300 pc,  $M_{300} \equiv M_{DM}(300 \text{ pc})$ .

Fig. 6 illustrates the analysis of the Markov chains of the galaxy IC 2574 by using GetDist code that is included in CosmoMC bayesian analysis code (Lewis & Bridle 2002). It is shown the posterior distributions of fitting ( $\rho_s$ ,  $r_s$ ) and derived parameters ( $\mu_{DM}$ ,  $M_{300}$ ) for the PISO, NFW, Spano, Burkert and Schive models. We will refer to these group of models as core-cusp group. Also, in Fig. 6, it is displayed the confidence region at  $1\sigma$  and  $2\sigma$ . We can notice the correlation between  $\mu_{DM}$  and  $r_s$  and the strong correlation between  $M_{300}$  and  $\rho_s$ . The pair  $M_{300}$  and  $\rho_s$  is anti correlated with the pair  $\mu_{DM}$  and  $r_s$ . We notice good Gaussian posteriors for the fitting parameters for all the models except for the NFW profile. As shown in Fig. 2 NFW is the worst fitting case for galaxy IC 2574.

In Figs. 7–9 are shown these four astrophysical observables ( $\rho_s$ ,  $r_s$ ,  $\mu_{DM}$  and  $M_{300}$ ) as a function of galaxy luminosity,  $L_{[3.6]}$ . From other studies it was expected that  $\mu_{DM}$  and  $M_{300}$  were nearly constant, independent of the absolute magnitude of the galaxies (Ureña-López et al. 2017; Kormendy & Freeman 2004; Strigari et al. 2008). The general tendency we found for the above four quantities is that  $\rho_s$  and  $M_{300}$  are roughly constant independently of the galaxy luminosity in the SPARC catalog except for the NFW model. We have found that a constant characteristic volume density of DM haloes is in agreement with Li et al. (2019). In agreement with (Strigari et al. 2008), we obtained that for dSph galaxies, the value of the mass is the same for spiral galaxies within 300 pc and with the same order of magnitude,  $\sim 10^7 M_\odot$ . This would give a central density for DM haloes of  $\sim 0.1 M_\odot \text{pc}^{-3}$  regardless the model, result not shared with NFW. Moreover, this result is consistent with both, non-parametric and parametric analysis, that are in favor of core models.

Theoretical and observational studies have given the result that the central surface density  $\mu_{DM}$  is constant inde-

pendently of the absolute magnitude of the galaxies (Ureña-López et al. 2017; Kormendy & Freeman 2004). We have obtained that this is not the case, and that  $\mu_{DM}$  grows linearly in the Log-Log scale as a function of  $L_{[3.6]}$ , fact that is in tension with previous results. Therefore, there is not a strong correlation between the density  $\rho_s$  and the scale  $r_s$  parameters for the density profiles we studied here, on the contrary,  $\rho_s$  is constant.

In Table 1 we show the compilation of the  $a$  and  $b$  parameters in the linear fit,  $a + bL$ , of the Log-Log scale of each one of the plots  $\rho_s$ ,  $r_s$ ,  $\mu_{DM}$  and  $M_{300}$  as a function of the luminosity  $L_{[3.6]}$ . For instance, we found that  $M_{300} \sim L^{0.03 \pm 0.04}$  for PISO model, that is the functional relationship found in Strigari et al. (2008). Similar behaviour is obtained for Spano, Burkert and Schive models. For the characteristic volume density we found a similar relation,  $\rho_s \sim L^{0.04 \pm 0.04}$  for PISO model and almost the same relations are found for Spano, Burkert and Schive. However, the relations for the scale length and the central surface density are  $r_s \sim L^{0.17 \pm 0.02}$  and  $\mu_{DM} \sim L^{0.18 \pm 0.02}$  for PISO and the same for the other models, except NFW which is the worst case as can be appreciated in Fig. 10 where we are illustrating the collection of all models in each plot. The  $1\sigma$  bands of the linear fit are also shown for comparison.

In Fig. 11 are displayed the expressions for the dimensionless mass and velocity functions of the core-cusp group (included in the Appendix A) and for a fixed scaling length  $r_s = 1$  and using the same value for  $r_s^3 \rho_s$  which is in units of mass. Figs. 10 and 11 show clearly the difference between core and cusp models. Additionally, from Fig. 11 it was shown that Spano and Schive models almost agree with each other even when Figs. 10(a) and (b) show clear differences between them for high luminosities. Up to  $2\sigma$  in the linear fit we may find an agreement between all core models nevertheless, there are clear differences at  $1\sigma$ . A detailed analysis following the cosmological method in Li et al. (2019) should clarify on this matter.

## 7 CONCLUSIONS

In this work we have performed a non parametric reconstruction of galactic rotation curves by using the LOESS+SIMEX technique as a method to discern between seven different DM models. Our main objective is to explain the DM contribution within the rotation curves of galaxies. In order to show the efficiency of LOESS+SIMEX and to report a quantitative result we have obtained the normalized area between the reconstructed curve and the fitted rotation curve, including also the area between  $1\sigma$  bands. Since we are comparing different models with different number of parameters, we use the AIC and BIC information criteria methods in order to assess the model fitness while penalizing the number of estimated parameters and, at the same time, giving support to LOESS+SIMEX results. Thus, to perform the model selection we use three conditions as a criterion to accept or reject models:

- $B_{\text{BIC}}$ : the best BIC value,
- $B_{\text{DIST}}$ : the area between the reconstructed curve and the rotation curve obtained with the best fit parameters, and

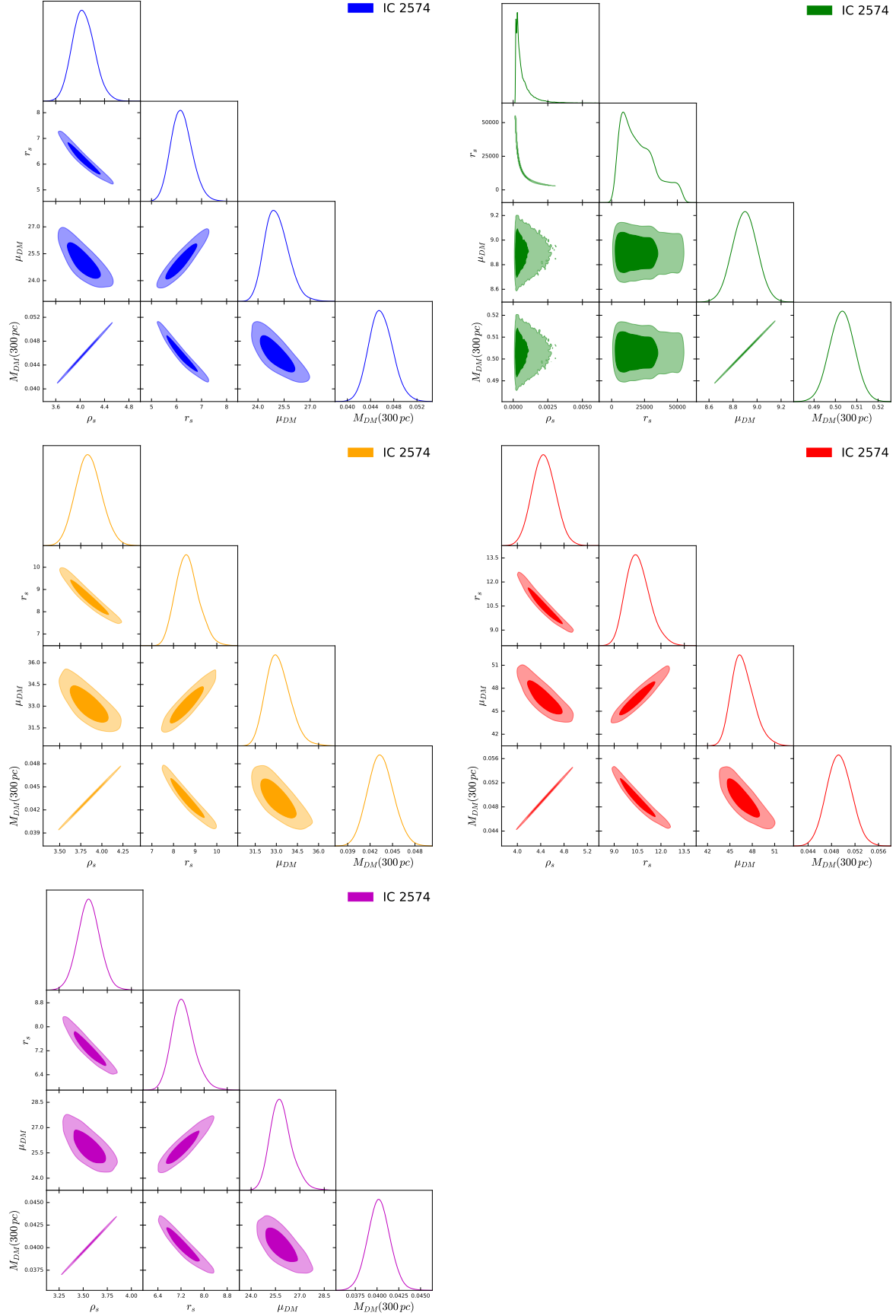


**Figure 6.** Posterior distributions for parameters  $\rho_s$ ,  $r_s$ ,  $\mu_{DM}$  and  $M_{300}$ . The contour lines are  $1\sigma$  and  $2\sigma$  confidence regions. From the top to right and to the bottom shown are PISO (blue), NFW (green), Spano (yellow), Burkert (red) and Schive (violet) models.



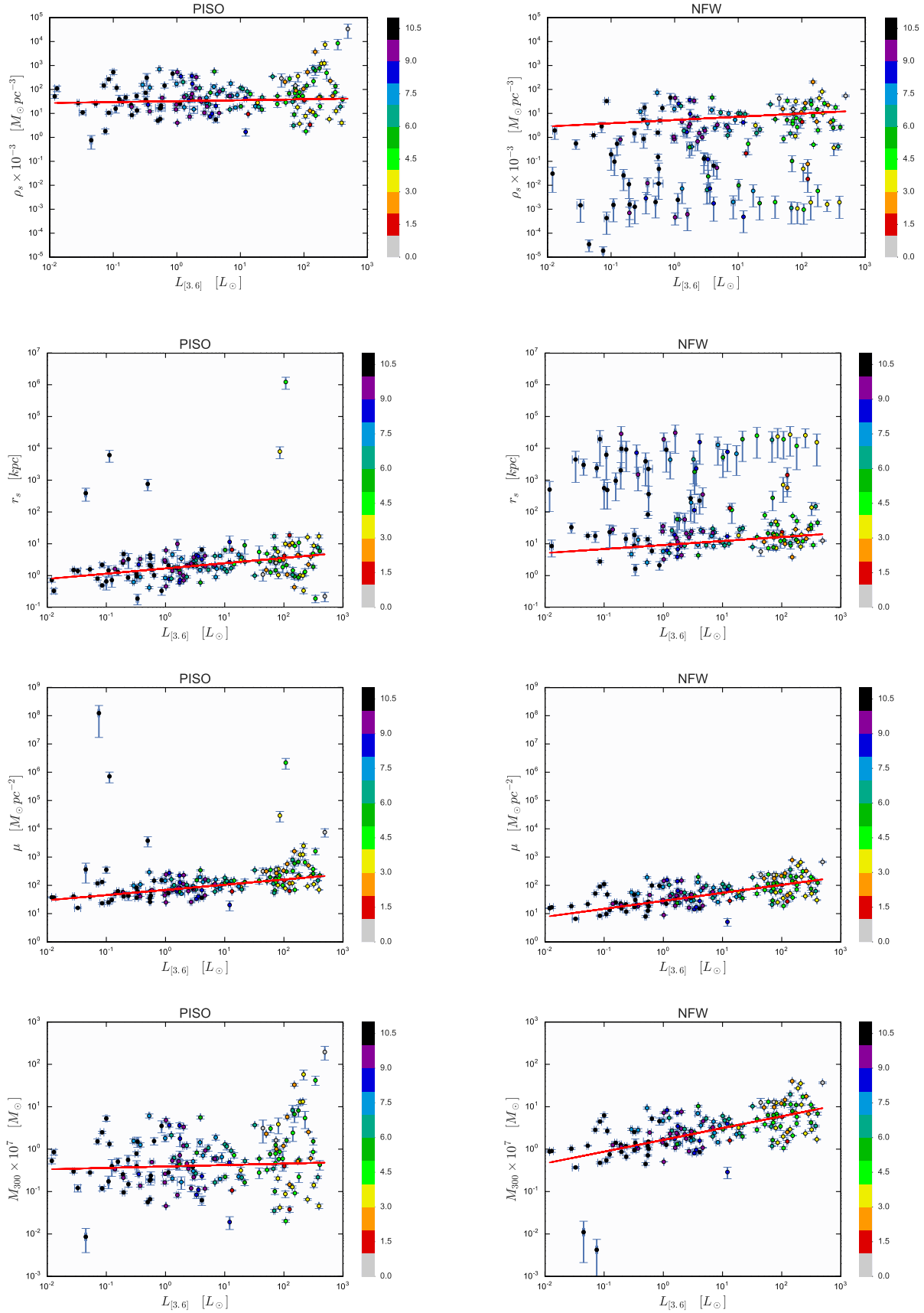


**Figure 7.** Shown are the characteristic volume density, the scale length, the characteristic central surface density and the mass within 300 pc as function of luminosity at 3.6  $\mu\text{m}$ . Left panel PISO, right panel NFW. Galaxies are colored by Hubble type with numbers from 0 to 11 corresponding to S0, Sa, Sab, Sb, Sbc, Sc, Scd, Sd, Sdm, Sm, Im, BCD, respectively. In all panels, solid lines show linear fits. MNRAS **000**, 1–19 (2018)

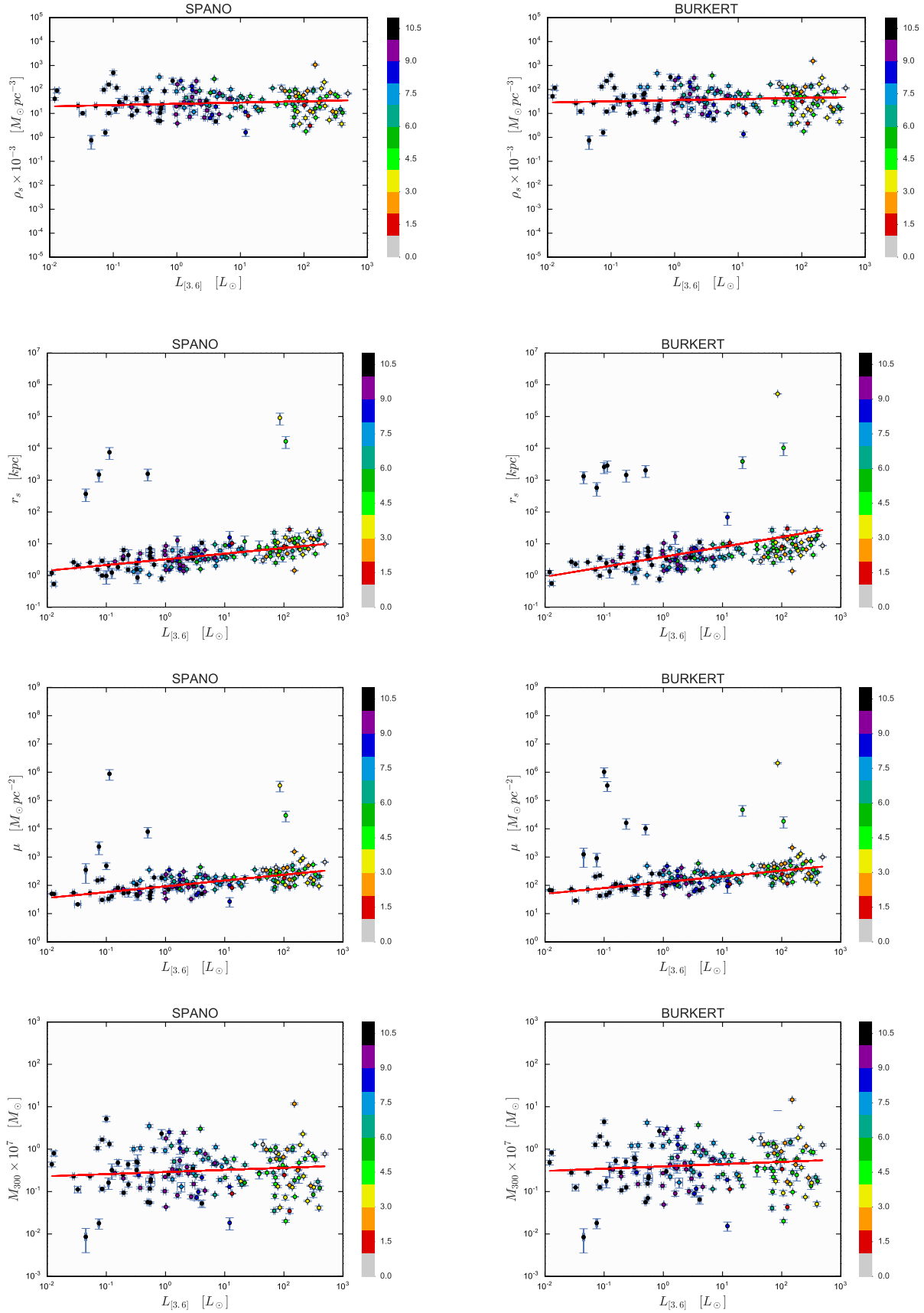


**Figure 8.** Shown are the characteristic volume density, the scale length, the characteristic central surface density and the mass within 300 pc as function of luminosity at  $3.6 \mu\text{m}$ . Left panel Spano, right panel Burkert. Galaxies are colored by Hubble type. In all panels, solid lines show linear fits. See caption of Fig 7.

Results compilation for the linear fit ( $a + b \log(L_{[3.6]})$ ) to SPARC galaxies observables						
		PISO	NFW	Spano	Burkert	Schive
$\rho_s$	$a$	$1.50966 \pm 0.07482$	$0.77526 \pm 0.09496$	$1.39718 \pm 0.06294$	$1.55027 \pm 0.06738$	$1.275 \pm 0.05622$
	$b$	$0.03908 \pm 0.04412$	$0.11217 \pm 0.05117$	$0.05472 \pm 0.03611$	$0.04798 \pm 0.0386$	$-0.0315 \pm 0.03317$
$r_s$	$a$	$0.22215 \pm 0.04073$	$0.94325 \pm 0.04649$	$0.51082 \pm 0.03099$	$0.5889 \pm 0.21369$	$0.55206 \pm 0.02854$
	$b$	$0.16663 \pm 0.02328$	$0.13417 \pm 0.02419$	$0.17885 \pm 0.01701$	$0.31454 \pm 0.11695$	$0.235 \pm 0.0161$
$\mu$	$a$	$1.83778 \pm 0.03038$	$1.44945 \pm 0.04341$	$1.96427 \pm 0.03031$	$2.10946 \pm 0.03356$	$1.86379 \pm 0.02744$
	$b$	$0.18341 \pm 0.01857$	$0.28382 \pm 0.02636$	$0.20559 \pm 0.01802$	$0.20571 \pm 0.02016$	$0.18314 \pm 0.01668$
$M_{DM}(300 \text{ pc})$	$a$	$-0.40992 \pm 0.07378$	$0.21738 \pm 0.04243$	$-0.54155 \pm 0.06218$	$-0.40713 \pm 0.06306$	$-0.66961 \pm 0.05572$
	$b$	$0.03284 \pm 0.04383$	$0.27863 \pm 0.02588$	$0.05115 \pm 0.03576$	$0.05376 \pm 0.03647$	$-0.03203 \pm 0.03291$

**Table 1.** Compilation of the results of the linear fit (log-log scale) parameters of  $\rho_s$ ,  $r_s$ ,  $\mu_{DM}$  and  $M_{DM}(300 \text{ pc})$ .

•  $B_{D1\sigma}$ : the area between the  $1\sigma$  reconstruction band and the  $1\sigma$  model fitting band.

We assign to each model a numerical code (1–4), which was ordered from the lowest value up to the highest one, according to any of the above requirements, indicating in the first place as the most preferred model by the data.

Furthermore, the DM models were separated in two groups (core + cusp and core + cusp + fuzzy models). In the first group we found that  $\sim 44.32\%$  of the galaxies satisfy the three conditions, where Spano is the most favored model with  $\sim 53.85\%$  while the NFW model is the least favored one, because is appearing in the last place according to the three conditions with the  $\sim 59\%$ . From the second group we found that Schive satisfies the three conditions in a  $44\%$ , while NFW turns out to be the rejected model with the  $21.6\%$  of the cases.

By performing a comparison between these three conditions, we are able to do a Core and Cusp classification for some of the galaxies which we have worked with. The DDO 064, DDO 168, F 571-v1, KK 98-251, NGC 6789, UGC 05986 and UGC 06399 are core type galaxies. On the other hand, NGC 0247, NGC 3741, UGC 05716, UGC 08490 and UGC 12732 can be classified as cusp galaxies. In some cases, when the FUZZY models were selected by one or more of the criteria used here, the corresponding transition radius turned out an important factor for the classification. The cases when  $r_e \sim r_{\min}$  pointing out to NFW as the best model to explain the structure of the galaxy; this showed that the LOESS+SIMEX method can be useful as technique of models selection.

To complement our analysis, by using a MCMC method, we have computed the haloes characteristic surface density,  $\rho_s r_s$  for each one of the DM models and also the DM mass within 300 pc. We obtained that there is a common mass for spiral galaxies of the order of  $10^7 M_\odot$ , result that is in agreement with ones of dSph Milky Way satellites. This would give a central density for the halo of  $\sim 0.1 M_\odot \text{ pc}^{-2}$  regardless the dark matter model. One extra result consistent with our findings is that there is a constant characteristic volume density of DM haloes:  $\rho_s$  is constant for the core models we analyzed. Moreover, we have found that characteristic central surface density is not constant for the SPARC galaxies, which is in tension with previous results, but in favor of core models which is in agreement with the non-parametric-parametric analysis.

Finally, we conclude that, in the study of galactic rotation curves, the non parametric LOESS+SIMEX method in combination with standard fitting methods turns out to be a reliable tool to perform DM models selection.

## ACKNOWLEDGEMENTS

L.M.F.H. acknowledges fruitful advice by S. McGaugh. All authors thank SNI-CONACYT for partial support. A.M. acknowledges support from postdoctoral grants from DGAPA-UNAM. M.A.R.M. acknowledges financial support from CONACyT project 283151, from “Fondo Sectorial de Investigación para la Educación”. All authors also thank to Juan Carlos Hidalgo, Nora Bretón and Luisa Jaime for reading the manuscript and for their helpful comments and suggestions.

## REFERENCES

- Alberto Vazquez J., Bridges M., Hobson M., Lasenby A., 2012, *JCAP*, 1209, 020
- Andersen R., 2009, *Annu. Rev. Sociol.*, 35, 67
- Azzalini A., Bowman A. W., Hardle W., 1989, *Biometrika*, 76, 1
- Begeman K. G., Broeils A. H., Sanders R. H., 1991, *Mon. Not. R. astr. Soc.*, 249, 523
- Bernal T., Fernández-Hernández L. M., Matos T., Rodríguez-Meza M. A., 2018, *Mon. Not. Roy. Soc.*, 475, 1447
- Bogdanos C., Nesseris S., 2009, *JCAP*, 0905, 006
- Bonvin C., Durrer R., Kunz M., 2006, *Phys.Rev.Lett.*, 96, 191302
- Burket A., 1995, *Astrophys. J. Lett.*, L25
- Carroll R., Ruppert D., Stefanski L., 1995, *The Measurement Error in Nonlinear Models. Monographs on Statistics and Applied Probability Series*, Chapman and Hall
- Carroll R. J., Maca J. D., Ruppert D., 1999, *Biometrika*, 86, 541
- Chen S.-R., Schive H.-Y., Chiueh T., 2017, *Mon. Not. Roy. Astron. Soc.*, 468, 1338
- Cleveland W., 1979, *J. Am. Statist. Assoc.*, 74, 82936
- Cleveland W., Devlin S. J., 1988, *J. Amer. Statist. Assoc.*, 83, 596
- Cook J. R., Stefanski L. A., 1994, *J. Amer. Statist. Assoc.*, 89, 1314
- Cousineau D., Allan T. A., 2015, *Mesure et évaluation en éducation*, 37, 63
- Einasto J., 1965, *Trudy Astrofizicheskogo Instituta Alma-Ata*, 5, 87
- Escamilla-Rivera C., Fabris J. C., 2016, *Galaxies*, 4, 76
- Espana-Bonet C., Ruiz-Lapuente P., 2005, *Phys.Rev.D*
- Feigelson E. D., Babu G. J., 2012, *Modern Statistical Methods for Astronomy*. Cambridge University Press, Cambridge, UK

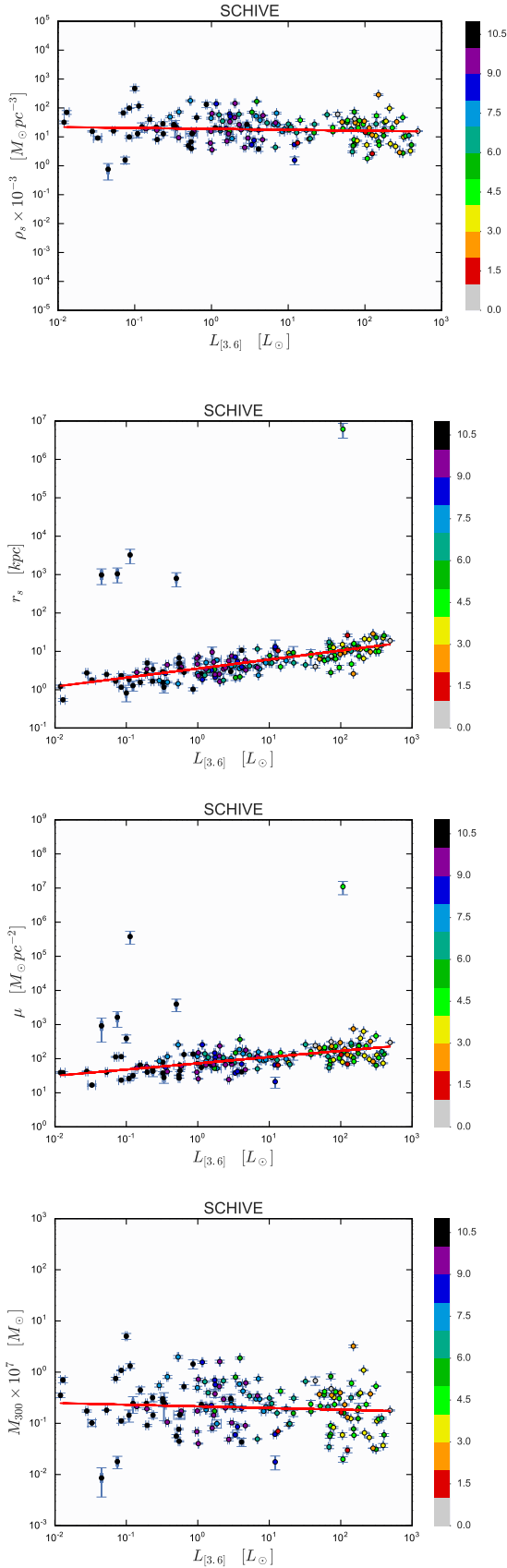


**Figure 9.** Shown are the characteristic volume density, the scale length, the characteristic central surface density and the mass within 300 pc as function of luminosity at 3.6  $\mu\text{m}$ . Schive model. Galaxies are colored by Hubble type. In all panels, solid lines show linear fits. See caption of Fig 7.

- Fox J., 2000, Nonparametric Simple Regression: Smoothing Scatterplots. No. 130 in Nonparametric Simple Regression: Smoothing Scatterplots, SAGE Publications
- Gamerman D., 1997, Markov Chain Monte Carlo: Stochastic Simulation for Bayesian Inference. Chapman & Hall/CRC Texts in Statistical Science, Taylor & Francis
- García-Aspeitia M. A., López-Domínguez J. C., Ortiz C., Hinojosa-Ruiz S., Rodríguez-Meza M. A., 2017, *Rev. Mex. Fis.*, 63, 423
- Gelman A., Rubin D. B., 1992, *Statistical Science*, 7, 457
- 2012, NIST/SEMATECH e-Handbook of Statistical Methods, <http://www.itl.nist.gov/div898/handbook/>
- Hernández-Almada A., García-Aspeitia M. A., 2018, *International Journal of Modern Physics D*, 27, 1850031
- Holsclaw T., Alam U., Sanso B., Lee H., Heitmann K., et al., 2010, *Phys.Rev.Lett.*, 105, 241302
- Huterer D., Starkman G., 2003, *Phys.Rev.Lett.*, 90, 031301
- Kormendy J., Freeman K. C., 2004, in Ryder S., Pisano D., Walker M., Freeman K., eds, IAU Symposium Vol. 220, Dark Matter in Galaxies. p. 377 ([arXiv:astro-ph/0407321](https://arxiv.org/abs/astro-ph/0407321))
- Lelli F., McGaugh S. S., Schombert J. M., 2016, *Astron. J.*, 152, 157
- Lelli F., McGaugh S. S., Schombert J. M., Pawłowski M. S., 2017, *ApJ*, 836, 152
- Lewis A., Bridle S., 2002, *Phys. Rev. D*, 66, 103511
- Li P., Lelli F., McGaugh S. S., Starkman N., Schombert J. M., 2019, *MNRAS*, 482, 5106
- McGaugh S. S., Lelli F., Schombert J. M., 2016, *Phys. Rev. Lett.*, 117, 201101
- Montiel A., Lazkoz R., Sendra I., Escamilla-Rivera C., Salzano V., 2014, *Phys. Rev.*, D89, 043007
- Navarro J. F., Frenk C. S., White S. D. M., 1996, *Astrophys. J.*, 462, 563
- Oh S.-H., et al., 2015, *AJ*, 149, 180
- Pontzen A., Governato F., 2014, *Nature*, 506, 171
- Press W., Teukolsky S. A., Vetterling W. T., Flannery B. P., 2007, Numerical Recipes. Cambridge University Press.
- Rana A., Jain D., Mahajan S., Mukherjee A., 2016, *JCAP*, 1607, 026
- Rani N., Jain D., Mahajan S., Mukherjee A., Pires N., 2015, *JCAP*, 1512, 045
- Schive H.-Y., Chiueh T., Broadhurst T., 2014, *Nature Physics*, 10, 496
- Schombert J., McGaugh S., 2014, *Publications of the Astronomical Society of Australia*, 31, e036
- Shafieloo A., Alam U., Sahni V., Starobinsky A. A., 2006, *Mon.Not.Roy.Astron.Soc.*, 366, 1081
- Shalizi C., 2012, Advanced Data Analysis from an Elementary Point of View
- Sofue Y., Rubin V., 2001, *Annu. Rev. Astron. Astrophys.*, 39, 137
- Spano M., Marcelin M., Amram P., Carignan C., Epinat B., Hernandez O., 2008, *Mon. Not. Roy. Astron. Soc.*, 383, 297
- Stefanski L., Cook J., 1995, *J. Amer. Statist. Assoc.*, 90, 1247
- Strigari L. E., Bullock J. S., Kaplinghat M., Simon J. D., Geha M., Willman B., Walker M. G., 2008, *Nature*, 454, 1096
- Ureña-López L. A., Robles V. H., Matos T., 2017, *Phys. Rev. D*, 96, 043005
- Wasserman L., 2006, All of Nonparametric Statistics. Springer, New York
- de Blok W. J. G., 2010, *Advances in Astronomy*, 2010, 789293
- de Blok W. J. G., Bosma A., 2002, *A&A*, 385, 816



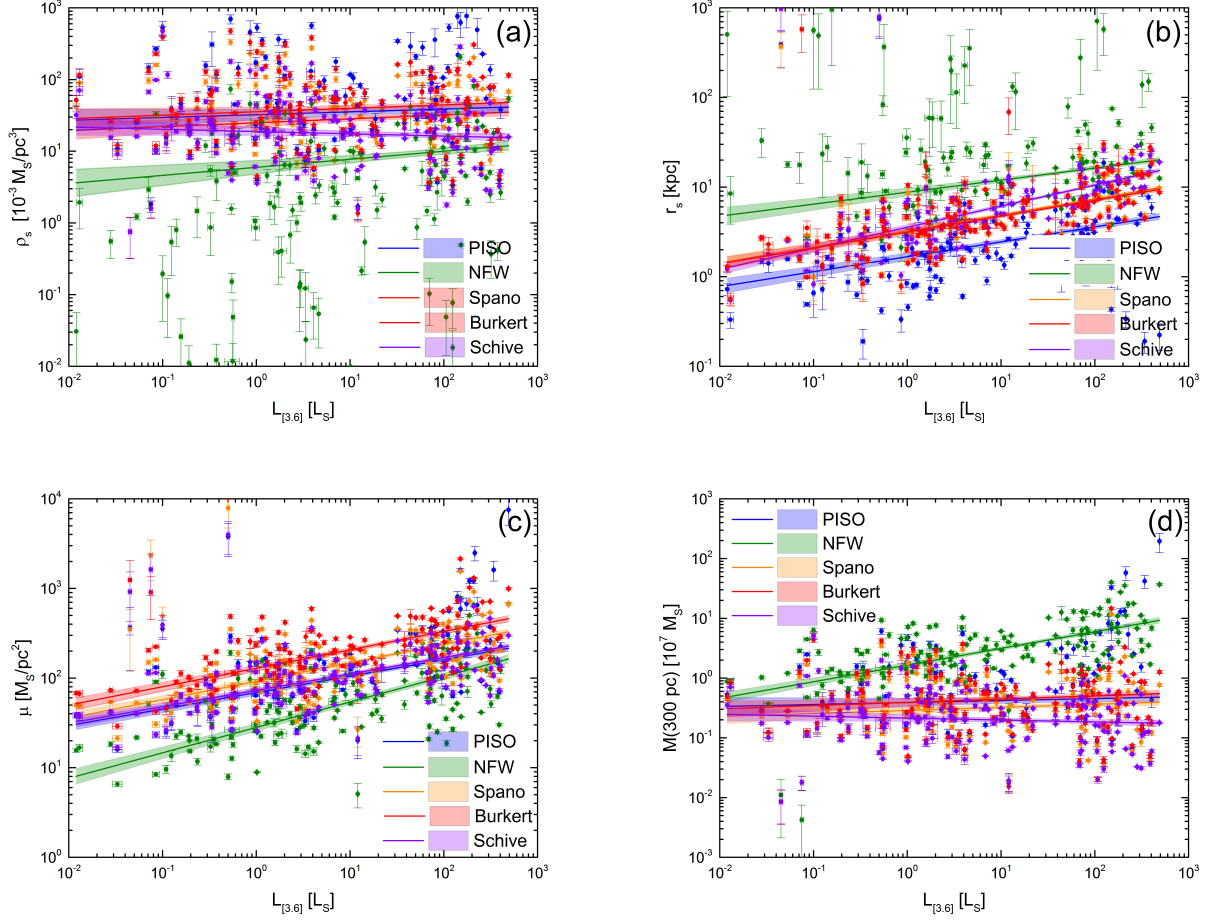


**Figure 10.** Same as Figs. 7–9 however we are illustrating all the models together and also displaying the fit and  $1\sigma$  bands of the linear (in Log-Log scale) fit.

## APPENDIX A: CORE, CUSP AND SFDM MODELS

Here we give a brief summary of the most common models in the literature reported in [Begeman et al. \(1991\)](#); [Navarro et al. \(1996\)](#); [Burket \(1995\)](#); [Spano et al. \(2008\)](#); [Chen et al. \(2017\)](#); [Bernal et al. \(2018\)](#). In general a rotation curve can be described by a general expression, see [Garcia-Aspeitia et al. \(2017\)](#) for more details

$$V_{model}^2(r) = 4\pi G r_{model} \mu_{model} \hat{V}_{model}^2(\hat{r}), \quad (\text{A1})$$

where  $\hat{V}(\hat{r})$  is a dimensionless function given by

$$\hat{V}(\hat{r}) = \sqrt{\frac{M(\hat{r})}{\hat{r}}}, \quad (\text{A2})$$

$\hat{r} = r/r_{model}$  with  $r_{model}$  being a length scale parameter for every model and  $\mu_{model} = \rho_{model} r_{model}$ , which is almost a constant when we fit observations but take a different value for each model ([Garcia-Aspeitia et al. 2017](#)). The dimensionless mass at a given radius  $\hat{r}$  is given by

$$M(\hat{r}) = 4\pi \int_0^{\hat{r}} dr' r'^2 \rho_{DM}(r'). \quad (\text{A3})$$

- (a) **Pseudo isothermal profile.** The DM density profile is written as:

$$\rho_{PISO}(r) = \frac{\rho_p}{1 + (r/r_p)^2}. \quad (\text{A4})$$

See [Begeman et al. \(1991\)](#) for more details. On the other hand, we can write the Eq. (A1), for PISO model as

$$\hat{V}_p^2(\hat{r}_p) = \frac{\hat{r}_p - \arctan(\hat{r}_p)}{\hat{r}_p}, \quad (\text{A5})$$

where  $\hat{r}_p = r/r_p$ .

- (b) **Navarro-Frenk-White profile.** Another interesting case (motivated by cosmological  $N$ -body simulations) is the cuspy NFW density profile which is given by [Navarro et al. \(1996\)](#):

$$\rho_{NFW}(r) = \frac{\rho_n}{(r/r_n)(1 + r/r_n)^2}, \quad (\text{A6})$$

where the dimensionless velocity for this model is

$$\hat{V}_{NFW}^2(\hat{r}_n) = \frac{1}{\hat{r}_n} \ln(1 + \hat{r}_n) - \frac{1}{1 + \hat{r}_n}, \quad (\text{A7})$$

and  $\hat{r}_n = r/r_n$  is defined using the scale radius  $r_n$ .

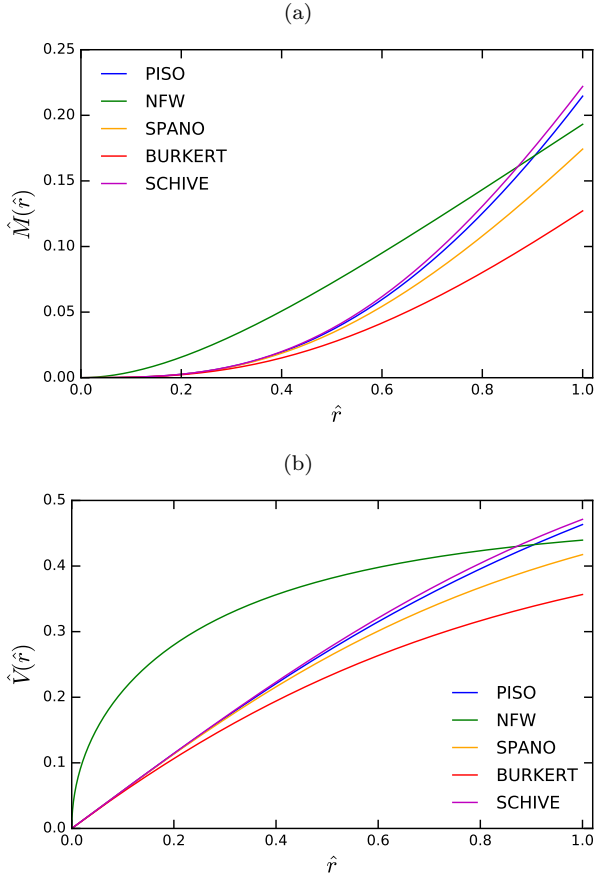


**Figure 11.** In (a) mass model for PISO, NFW, Spano, Burkert and Schive DM models.  $\hat{M}$  and  $\hat{r}$  are dimensionless quantities defined in Appendix A. In (b) velocity model for the same DM models as in (a).  $\hat{V}$  is also a dimensionless velocity defined in Appendix A.

- (c) **Burkert profile.** Another core density profile proposed by Burkert (1995) is:

$$\rho_{\text{Burk}} = \frac{\rho_b}{(1 + r/r_b)(1 + (r/r_b)^2)}, \quad (\text{A8})$$

with the above density profile we have

$$\hat{V}_{\text{Burk}}^2(\hat{r}_b) = \frac{1}{4\hat{r}_b} \left( -2 \arctan(\hat{r}_b) + \ln \left[ (1 + \hat{r}_b^2)(1 + \hat{r}_b)^2 \right] \right). \quad (\text{A9})$$

- (d) **Spano profile.** The density profile proposed by Spano et al. (2008) is

$$\rho_{\text{Spano}} = \frac{\rho_{sp}}{(1 + (r/r_{sp})^2)^{3/2}}, \quad (\text{A10})$$

we obtain a dimensionless quantity given by

$$\hat{V}_{\text{sp}}^2(\hat{r}_{sp}) = -\frac{1}{\sqrt{1 + \hat{r}_{sp}^2}} + \frac{1}{\hat{r}_{sp}} \operatorname{arcsinh}(\hat{r}_{sp}). \quad (\text{A11})$$

- (e) **Schive profile.** Here we consider that DM density profile is given by WaveDM density profile, see Schive et al.

(2014); Bernal et al. (2018):

$$\rho_{\text{WDM}}(r) = \frac{\rho_w}{(1 + a_w(r/r_w)^2)^8}, \quad (\text{A12})$$

where  $a_w = 0.091$ . Then, if we define  $\hat{r}_w = r/r_w$ , it is obtained

$$\begin{aligned} \hat{V}_w^2(\hat{r}_w) = & \frac{1}{215040a_w^{3/2}} \left[ \frac{a_w^{1/2}}{(1 + a_w\hat{r}_w^2)^7} (-3465 \right. \\ & + 48580a_w\hat{r}_w^2 + 92323a_w^2\hat{r}_w^4 + 101376a_w^3\hat{r}_w^6 \\ & + 65373a_w^4\hat{r}_w^8 + 231000a_w^5\hat{r}_w^{10} + 3465a_w^6\hat{r}_w^{12}) \\ & \left. - 3465 \arctan(\sqrt{a_w}\hat{r}_w) \right]. \quad (\text{A13}) \end{aligned}$$

- (f) **Wave+NFW (SNFW) with continuity condition in the density profile.** In this subsection we consider the DM profile motivated by simulations where the DM can be modeled with a Scalar Field (Schive et al. 2014), using the expression for density profile for the core Eq. (A12) and the Eq. (A6) for the cuspy we obtain

$$\begin{aligned} \rho_{\text{SNFWC}}(r) = & \Theta(r_\epsilon - r) \rho_{\text{WDM}}(r) \\ & + \Theta(r - r_\epsilon) \rho_{\text{NFW}}(r), \quad (\text{A14}) \end{aligned}$$

with the continuity condition on the density profiles at the matching radius  $r_\epsilon$ ,  $\rho_{\text{WDM}}(r_\epsilon) = \rho_{\text{NFW}}(r_\epsilon)$ . With this condition we have four free parameters  $r_w$ ,  $r_\epsilon$ ,  $r_n$  and  $\rho_w$ , Eqs. (A7, A13). Then we can write the velocity rotation curve as Bernal et al. (2018)

$$\begin{aligned} \hat{V}_{\text{SNFWC}}^2(\hat{r}_w, \hat{r}_\epsilon, \hat{r}_n) = & \begin{cases} \hat{V}_{\text{WDM}}(\hat{r}_w) & \text{if } \hat{r}_w \leq \frac{\hat{r}_w}{\hat{r}_\epsilon}, \\ \hat{V}_{\text{WDM}}(\frac{\hat{r}_w}{\hat{r}_\epsilon}) - \hat{V}_{\text{NFW}}(\frac{\hat{r}_n}{\hat{r}_\epsilon}) + \hat{V}_{\text{NFW}}(\hat{r}_n) & \text{if } \hat{r}_n > \frac{\hat{r}_n}{\hat{r}_\epsilon} \end{cases} \end{aligned}$$

- (g) **Wave+NFW (SNFW) with continuity condition on the density profile and on its derivative.**

This case was proposed in Bernal et al. (2018). Here we consider the same density profile Eq. (A14), the continuity condition  $\rho_{\text{WDM}}(r_\epsilon) = \rho_{\text{NFW}}(r_\epsilon)$  and a differentiable continuity condition at the transition radius  $r_\epsilon$ ,  $\rho'_{\text{WDM}}(r_\epsilon) = \rho'_{\text{NFW}}(r_\epsilon)$ . With these conditions we have only three free parameters  $r_w$ ,  $r_\epsilon$  and  $\rho_w$ , where

$$\begin{aligned} \hat{V}_{\text{SNFWDC}}^2(\hat{r}_w, \hat{r}_\epsilon) = & \begin{cases} \hat{V}_{\text{WDM}}(\hat{r}_w) & \text{if } \hat{r}_w \leq \frac{\hat{r}_w}{\hat{r}_\epsilon}, \\ \hat{V}_{\text{WDM}}(\frac{\hat{r}_w}{\hat{r}_\epsilon}) - \hat{V}_{\text{NFW}}(\frac{\hat{r}_n}{\hat{r}_\epsilon}) + \hat{V}_{\text{NFW}}(\hat{r}_n) & \text{if } \hat{r}_n > \frac{\hat{r}_n}{\hat{r}_\epsilon}. \end{cases} \end{aligned}$$

**APPENDIX B: COMPARISON PARAMETRIC  
VERSUS NON-PARAMETRIC TABLES**

This paper has been typeset from a  $\text{\LaTeX}$  file prepared by the author.

MNRAS **000**, 1–19 (2018)



SPARC Galaxies Statistics																																
Galaxy	FISO (1)					NTF (2)					SPAN0 (3)					BURKERT (4)					BEST MODEL											
	$P$ -Value	AIC	BIC	DIST	$\chi^2_{red}$	$P$ -Value	AIC	DIST	$\chi^2_{red}$	$\chi^2_{red}$	$P$ -Value	AIC	BIC	DIST	$\chi^2_{red}$	$P$ -Value	AIC	BIC	DIST	$\chi^2_{red}$	$B_{cut}$	$B_{best}$	$B_{size}$	$B_{size}$	$P$ -Value	AIC	BIC	DIST	$\chi^2_{red}$	$B_{cut}$	$B_{best}$	$B_{size}$
1	2	3	4	5	6	7	8	9	10	11	12	13	14	15	16	17	18	19	20	21	22	23	24	25	26	27	28	29	30			
DDO 161	0.33	0.00030	113.83	123.56	0.28	0.22	1.15	0.73	137.44	147.18	0.36	0.50	0.25	0.000015	111.46	121.20	0.25	0.19	0.27	0.000026	111.81	121.55	0.27	0.21	3412	3412	3412	3412	3412	3412	3412	3412
563-1	0.56	0.0095	18726.84	18734.41	0.29	0.22	1.15	0.62	16230.84	16238.17	0.30	0.23	0.55	0.0088	23179.41	23179.41	0.28	0.22	0.56	0.0095	23021.41	23028.75	0.28	0.22	2143	3412	3412	3412	3412	3412	3412	3412
563-2	0.29	0.0310	51926.01	51931.22	0.30	0.21	1.23	0.775	50903.70	50909.00	0.44	0.33	0.11	0.00021	42960.47	42965.68	0.20	0.15	0.18	0.0062	44883.91	44889.12	0.23	0.17	3412	3412	3412	3412	3412	3412	3412	3412
568-1	0.14	0.00082	53895.17	53901.11	0.17	0.07	0.86	0.429	63193.03	6324.97	0.27	0.13	0.07	0.000023	55216.03	55221.97	0.15	0.10	0.10	0.00018	56252.44	56252.44	0.15	0.11	3412	3412	3412	3412	3412	3412	3412	3412
571-8	10.75	1.00000	61560.53	61569.79	0.88	0.65	19.17	1.0000	54591.23	54957.49	1.20	0.93	10.22	1.00	61933.64	61945.90	0.80	0.62	10.84	1.0000	61554.34	61560.60	0.86	0.64	2143	3412	3412	3412	3412	3412	3412	3412
579-1	0.05	$5.0 \times 10^{-7}$	33553.33	33559.89	0.18	0.06	0.19	0.00108	33342.86	33349.41	0.18	0.12	0.37	0.027	30594.21	30600.77	0.26	0.16	0.25	0.0049	31124.25	31130.80	0.22	0.15	3421	3412	3412	3412	3412	3412	3412	3412
GC 1003	3.34	1.000	255.13	265.46	0.46	0.28	2.57	1.0000	229.02	239.36	0.45	0.31	6.56	1.000	364.76	375.10	0.78	0.55	5.54	1.0000	330.25	340.58	0.69	0.47	2143	3412	3412	3412	3412	3412	3412	3412
GC 2015	0.70	0.120	202.07	211.68	0.36	0.21	0.96	0.47	209.31	218.92	0.39	0.27	0.53	0.021	197.48	207.08	0.32	0.20	0.56	0.031	198.28	207.88	0.33	0.21	3412	3412	3412	3412	3412	3412	3412	3412
GC 2076	0.30	0.00024	127.00	136.18	0.23	0.22	1.90	0.9857	167.08	176.27	0.54	0.24	0.29	0.00023	128.95	136.14	0.23	0.22	0.30	0.00032	127.21	136.40	0.24	0.22	3412	3412	3412	3412	3412	3412	3412	3412
GC 2081	0.26	0.00008	133.07	141.95	0.21	0.16	1.30	0.8278	157.46	166.34	0.37	0.32	0.20	0.00001	132.08	140.95	0.34	0.25	0.57	0.160	138.19	142.06	0.21	0.15	3412	3412	3412	3412	3412	3412	3412	3412
GC 0128	0.73	0.181	150.26	159.13	0.28	0.22	1.47	0.0324	167.28	176.16	0.43	0.37	0.74	0.193	150.50	159.37	0.28	0.22	0.68	0.133	170.59	158.04	0.27	0.22	4312	3412	3412	3412	3412	3412	3412	3412
GC 0478	0.27	0.0018	29.15	33.47	0.28	0.23	0.59	0.264	31.09	35.41	0.32	0.32	0.23	0.034	28.93	33.25	0.28	0.23	0.25	0.040	29.02	33.60	0.24	0.21	4312	3412	3412	3412	3412	3412	3412	3412
GC 0483	0.27	$10^{-9}$	78.18	83.77	0.19	0.12	0.22	0.0079	79.85	85.44	0.18	0.11	0.01	$4.0 \times 10^{-8}$	78.00	83.59	0.21	0.14	0.01	$5.0 \times 10^{-8}$	78.01	83.60	0.21	0.13	2134	3412	3412	3412	3412	3412	3412	3412
GC 0505	0.03	$3.0 \times 10^{-7}$	40.19	45.72	0.28	0.20	0.89	0.328	42.81	48.39	0.36	0.36	0.13	0.028	26.30	29.47	0.31	0.27	0.09	0.014	26.14	29.30	0.30	0.28	4312	3412	3412	3412	3412	3412	3412	3412
GC 0514	0.60	0.014	26.15	29.32	0.30	0.28	1.05	0.619	29.98	33.14	0.37	0.36	0.13	0.028	26.30	29.47	0.31	0.27	0.09	0.014	26.14	29.30	0.30	0.28	4312	3412	3412	3412	3412	3412	3412	3412
GC 0521	0.81	0.290	137.23	145.77	0.36	0.20	0.96	0.449	140.45	148.99	0.37	0.20	0.42	0.01	129.04	137.58	0.22	0.13	0.39	0.060	128.46	137.00	0.21	0.14	4312	3412	3412	3412	3412	3412	3412	3412
GC 0570	0.17	0.0031	71.06	76.65	0.16	0.18	1.00	0.57	78.57	84.16	0.25	0.16	0.07	0.00011	70.20	75.79	0.15	0.18	0.12	0.00071	70.59	76.18	0.21	0.19	3412	3412	3412	3412	3412	3412	3412	3412
GC 0572	0.15	0.0018	66.82	72.43	0.21	0.16	0.09	0.00021	60.67	66.27	0.19	0.16	0.26	0.015	62.22	67.81	0.22	0.18	0.20	0.0054	61.65	67.25	0.20	0.17	2143	3412	3412	3412	3412	3412	3412	3412
GC 0618	1.17	0.681	51.84	56.15	0.34	0.28	3.55	0.998	66.12	70.44	0.65	0.36	1.16	0.678	51.80	56.12	0.34	0.28	1.21	0.703	52.08	56.40	0.34	0.27	3412	3412	3412	3412	3412	3412	3412	3412
GC 0617	0.27	0.0163	57.68	63.27	0.21	0.17	0.80	0.387	62.52	68.11	0.30	0.14	0.19	0.005	57.01	62.60	0.21	0.19	0.20	0.053	57.05	62.64	0.19	0.20	3412	3412	3412	3412	3412	3412	3412	3412
GC 0623	0.51	0.273	37.03	40.19	0.32	0.34	0.95	0.37	38.80	41.96	0.36	0.35	0.42	0.209	36.67	39.84	0.33	0.33	0.48	0.251	36.91	40.07	0.33	0.32	3412	3412	3412	3412	3412	3412	3412	3412
GC 0693	0.46	0.041	101.41	108.75	0.28	0.27	0.60	0.120	103.40	110.73	0.27	0.27	0.47	0.044	101.52	108.85	0.18	0.29	0.42	0.027	100.80	108.13	0.20	0.28	4312	3412	3412	3412	3412	3412	3412	3412
GC 0708	0.16	0.00139	66.49	72.43	0.21	0.11	0.27	0.0119	61.57	73.51	0.22	0.16	0.10	0.003	66.75	72.69	0.23	0.12	0.15	0.00115	66.42	72.36	0.21	0.11	4312	3412	3412	3412	3412	3412	3412	3412
GC 0725	0.46	0.072	57.34	63.60	0.35	0.19	0.85	0.411	61.67	67.93	0.42	0.24	0.23	0.003	54.77	60.91	0.23	0.12	0.25	0.0060	54.99	61.25	0.25	0.13	3412	3412	3412	3412	3412	3412	3412	3412
GC 0751	1.05	0.60	54.29	59.88	0.37	0.27	2.86	0.908	70.63	76.23	0.47	0.29	0.76	0.347	51.71	57.30	0.29	0.31	0.85	0.43	52.54	58.14	0.30	0.32	3412	3412	3412	3412	3412	3412	3412	3412
GC 0752	0.11	0.011	21.13	22.67	0.22	0.26	2.41	0.911	25.73	27.28	0.54	0.27	0.11	0.07	21.13	22.67	0.22	0.26	0.12	0.11	21.14	22.68	0.23	0.26	3412	3412	3412	3412	3412	3412	3412	3412
GC 0761	0.09	0.006	41.58	45.37	0.21	0.15	0.05	0.0014	41.38	45.16	0.20	0.13	0.50	0.223	43.63	47.41	0.28	0.21	0.37	0.132	43.00	46.78	0.26	0.20	2143	3412	3412	3412	3412	3412	3412	3412
GC 0723	0.32	0.042	52.01	57.22	0.21	0.10	0.71	0.316	55.11	60.32	0.37	0.26	0.33	0.005	49.79	57.30	0.21	0.11	0.30	0.0021	51.80	57.01	0.21	0.10	4312	3412	3412	3412	3412	3412	3412	3412
GC 0759	0.08	0.008	33.79	37.57	0.21	0.17	0.43	0.171	35.42	39.20	0.25	0.24	0.08	0.005	33.69	37.48	0.21	0.17	0.10	0.008	33.79	37.57	0.21	0.17	3412	3412	3412	3412	3412	3412	3412	3412
GC 0757	0.8	0.0008	41.87	46.65	0.22	0.08	0.20	0.0153	42.74	47.53	0.26	0.10	0.08	0.0008	41.87	46.66	0.22	0.08	0.08	0.0009	41.89	46.68	0.22	0.08	1342	3412	3412	3412	3412	3412	3412	3412
GC 0760	0.40	0.154	39.34	43.12	0.23	0.07	0.34	0.108	39.03	42.78	0.20	0.08	0.08	0.005	37.72	41.51	0.18	0.12	0.11	0.011	37.87	41.66	0.18	0.11	3421	3412	3412	3412	3412	3412	3412	3412
GC 0766	0.05	0.0012	36.75	40.53	0.21	0.16	0.04	0.0011	36.73	40.52	0.19	0.18	0.09	0.006	36.95	40.73	0.21	0.17	0.07	0.032	36.86	40.64	0.21	0.17	2134	3412	3412	3412	3412	3412	3412	3412
GC 0832	0.67	0.325	37.29	41.61	0.26	0.27	6.33	1.00	71.27	75.59	0.88	0.52	0.68	0.332	37.34	41.66	0.26	0.27	0.77	0.408	37.91	42.23	0.29	0.25	1243	3412	3412	3412	3412	3412	3412	3412
GC 0897	0.008	0.001	30.55	32.98	0.20	0.19	0.01	0.002	30.56	33.00	0.21	0.19	0.03	0.007	30.62	33.05	0.22	0.18	0.02	0.005	30.60	33.03	0.22	0.18	1243	3412	3412	3412	3412	3412	3412	3412
GC 10310	0.27	0.069	40.90	44.68	0.22	0.10	0.57	0.276	42.41	46.19	0.25	0.09	0.06	0.002	39.85	43.63	0.18	0.11	0.09	0.007	40.03	43.82	0.18	0.12	3412	3412	3412	3412	3412	3412	3412	3412
GC 1444	5.95	$1.0 \times 10^{-8}$	84.50	89.71	2.36	2.04	1.33	0.778	47.54	52.75	1.38	1.79	8.67	1.00	106.21	111.42	2.64	2.33	7.56	1.00	97.34	102.55	2.54	2.24	2143	3412	3412	3412	3412	3412	3412	3412
GC A44	0.20	$9.0 \times 10^{-8}$	172.24	182.58	0.17	0.12	0.06	$1.7 \times 10^{-15}$	167.64	177.97	0.16	0.09	0.																			

Table B1. Continue.

Galaxy	$\delta A_V$	SCHIVE (1)					NFW (2)					SNFWDC (3)					SNFWC (4)					BEST MODEL								
		$\chi^2_{red}$	$P$ -Value	AIC	BIC	DIST	$\chi^2_{red}$	$P$ -Value	AIC	BIC	DIST	$\chi^2_{red}$	$P$ -Value	AIC	BIC	DIST	$\chi^2_{red}$	$P$ -Value	AIC	BIC	DIST	$B_{best}$	$B_{1\sigma}$	$B_{2\sigma}$	$B_{3\sigma}$					
1		2	3	4	5	6	7	8	9	10	11	12	13	14	15	16	17	18	19	20	21	22	23	24	25	26	27	28	29	30
D 512-2*	46.3	0.08	0.07	21.93	23.48	0.32	0.47	0.31	0.27	0.22	22.41	23.95	0.29	0.48	0.09	0.24	23.87	26.19	0.19	0.73	–	–	25.87	28.96	0.31	0.77	1.234	2(34)1	1234	1324
D 564-8	43.9	0.04	0.003	21.82	24.98	0.26	0.26	0.91	0.55	25.30	28.47	0.22	0.36	0.04	0.009	0.009	23.75	28.50	0.25	0.35	0.08	0.08	25.82	32.15	0.26	0.31	1.234	23(14)	1432	(134)2
D 631-7	49.1	0.75	0.280	70.75	77.84	0.33	0.25	6.04	1.000	144.79	151.88	0.79	0.59	0.81	0.35	72.75	83.38	0.33	0.25	0.60	0.156	71.38	85.56	0.25	0.16	1.234	4(13)2	(134)2	4132	
DDO 064	49.7	0.27	0.0066	77.97	84.52	0.22	0.16	0.56	0.124	81.42	87.98	0.30	0.31	0.30	0.0132	79.97	89.80	0.22	0.16	0.33	0.0255	81.97	95.08	0.22	0.16	1.234	(134)2	(1234)	1342	
DDO 154	41.9	2.00	0.971	29.33	35.27	0.38	0.26	11.77	1.000	127.05	132.99	1.86	1.55	1.24	0.73	22.49	31.40	0.43	0.47	1.39	0.807	24.49	36.37	0.43	0.49	3142	1(34)2	1342	3412	
DDO 168	56.0	3.32	0.999	60.30	65.51	0.61	0.35	10.69	1.00	119.26	124.47	1.05	0.64	0.39	1.00	62.30	70.11	0.61	0.35	4.43	1.00	64.30	74.72	0.61	0.39	1.342	(134)2	(134)2	1342	
DDO 170	49.4	6.20	1.00	60.01	64.33	0.75	0.42	2.16	0.956	35.76	40.08	0.64	0.57	1.45	0.80	32.06	38.54	0.55	0.41	0.48	0.246	28.69	37.33	0.47	0.54	4321	4321	4321	4321	
ESO 116-G012	50.0	1.42	0.86	82.96	89.79	0.34	0.33	2.35	0.9961	95.06	101.89	0.60	0.28	1.03	0.584	78.89	89.14	0.24	0.46	1.13	0.66	80.89	94.56	0.24	0.48	3412	(34)12	2134	3412	
ESO 444-G084	34.7	3.87	0.998	50.00	53.78	0.36	0.23	0.67	0.354	33.98	37.76	0.35	0.24	0.17	0.047	33.31	38.99	0.35	0.19	0.23	0.123	35.31	42.88	0.35	0.28	2341	(234)1	3124	3412	
F 565-V2	36.0	0.05	0.0017	44.82	48.60	0.18	0.12	0.37	0.133	46.42	50.21	0.25	0.20	0.03	0.002	46.68	52.36	0.19	0.17	0.02	0.004	48.62	56.19	0.17	0.31	1.234	4132	1324	4312	
F 568-3	46.2	0.90	0.435	126.48	134.04	0.34	0.20	3.20	1.000	163.19	170.75	0.29	0.14	0.76	0.276	125.41	136.76	0.26	0.14	0.71	0.232	126.94	141.06	0.23	0.13	1.342	4321	4(23)1	4312	
F 568-V1	36.4	0.43	0.042	115.98	122.81	0.29	0.20	0.22	0.00154	113.19	120.02	0.35	0.24	0.06	2.4 $\times 10^{-6}$	113.08	123.33	0.23	0.15	0.07	1.0 $\times 10^{-5}$	115.08	128.74	0.23	0.13	2134	(34)12	4312	3421	
F 571-V1	45.7	0.09	0.006	44.73	48.52	0.23	0.24	0.24	0.098	45.90	49.68	0.26	0.27	0.01	0.0002	46.35	52.02	0.25	0.31	0.008	0.0009	48.32	55.89	0.25	0.36	1.234	1(34)2	1234	4312	
F 574-1	42.7	0.78	0.330	81.70	88.26	0.31	0.24	1.64	0.928	92.04	98.60	0.43	0.26	0.03	2.0 $\times 10^{-7}$	74.65	84.49	0.23	0.21	0.02	7.0 $\times 10^{-8}$	76.51	89.63	0.23	0.24	3142	(34)12	3(14)2	4312	
F 583-1	40.1	0.28	0.00039	151.42	160.29	0.27	0.18	1.60	0.9661	181.73	190.61	0.40	0.29	0.11	6.0 $\times 10^{-8}$	149.29	162.61	0.20	0.08	0.11	1.7 $\times 10^{-7}$	151.28	169.03	0.20	0.11	1.342	(34)12	3412	(34)12	
F 583-4	40.6	1.04	0.591	74.39	80.33	0.30	0.29	0.15	0.00112	65.54	71.48	0.24	0.33	0.14	0.0014	67.28	76.19	0.24	0.34	0.16	0.0039	69.28	81.15	0.25	0.41	2341	(234)1	1234	3241	
IC 2574	49.8	3.49	1.000	228.11	238.22	0.17	0.1	33.54	1.000	1189.77	1199.88	0.49	0.36	1.31	0.8845	158.98	174.14	0.24	0.14	3.40	1.000	222.26	242.47	0.14	0.14	3142	4132	(134)2	3412	
KK 98-251	61.4	0.23	0.0022	55.39	62.23	0.25	0.09	1.82	0.9658	76.05	82.88	0.56	0.34	0.25	0.0047	57.39	67.64	0.25	0.09	0.28	0.0007	59.39	73.06	0.25	0.09	1.342	(134)2	(134)2	1342	
NGC 0024	28.3	3.34	1.000	262.10	271.57	1.12	0.92	0.83	0.43	196.93	206.40	0.31	0.24	0.44	0.0057	185.14	199.34	0.36	0.24	0.21	8.8 $\times 10^{-6}$	181.02	199.96	0.11	0.20	3421	4231	4(23)1	4321	
NGC 0055	61.2	0.13	2.1 $\times 10^{-6}$	96.56	104.73	0.22	0.12	2.97	1.000	150.50	158.68	0.45	0.35	0.13	4.5 $\times 10^{-6}$	98.48	110.74	0.21	0.09	0.12	3.3 $\times 10^{-6}$	100.09	116.44	0.20	0.07	1.342	4312	4312	4(13)2	
NGC 0100	52.4	0.18	0.00035	114.92	123.10	0.22	0.17	0.77	0.250	126.00	134.18	0.36	0.28	0.06	6.5 $\times 10^{-9}$	114.52	126.79	0.22	0.13	0.06	2.1 $\times 10^{-8}$	116.49	132.85	0.21	0.11	1.342	4(13)2	4312	(34)12	
NGC 0247	49.3	14.10	1.0000	458.10	467.13	0.96	0.78	1.85	0.9931	164.15	173.18	0.22	0.14	1.27	0.83	150.95	164.50	0.20	0.16	1.32	0.856	152.78	170.84	0.20	0.16	3421	(34)21	2(34)1	3421	
NGC 0300	44.7	1.80	0.9896	175.20	184.07	0.42	0.35	0.65	0.101	148.58	157.46	0.30	0.23	0.41	0.0008	144.72	158.03	0.28	0.19	0.41	0.0005	146.22	163.97	0.22	0.12	2341	4321	4321	4321	
NGC 3109	36.2	0.37	0.0027	104.33	113.20	0.22	0.16	8.55	1.0000	292.53	301.40	0.69	0.50	0.22	0.000047	102.62	115.93	0.17	0.1	0.23	0.000101	104.62	122.37	0.17	0.13	1.342	(34)12	3412	3412	
NGC 3741	32.2	2.29	0.9899	120.87	129.05	0.51	0.30	0.34	0.0037	83.98	92.16	0.20	0.20	0.36	0.0057	85.84	98.11	0.19	0.21	0.37	0.0083	87.65	104.01	0.20	0.23	2341	3(24)1	2341	2341	
NGC 6789*	49.2	0.30	0.26	24.68	26.23	0.23	0.16	2.04	0.870	28.16	29.71	0.45	0.21	1.18	0.33	26.26	28.58	0.24	0.36	–	–	28.68	31.77	0.23	0.34	1.324	3124	3124	3124	
UGC 00091	40.6	27.75	1.000	225.28	230.06	1.03	0.94	3.38	0.999	56.09	59.69	0.87	0.93	0.78	1.89	0.922	44.35	51.33	0.74	0.56	1.16	0.67	40.78	50.36	0.36	0.41	4321	4132	4132	4132
UGC 04693	42.7	1.34	0.737	19.51	21.06	1.01	1.07	3.20	0.959	23.24	24.79	1.20	0.88	0.68	0.59	19.52	21.84	0.99	1.50	–	–	21.52	24.61	0.99	1.46	1.342	(34)12	(34)12	3124	
UGC 06834*	47.0	0.61	0.392	15.47	17.80	0.21	0.14	3.10	0.974	22.94	25.38	0.71	0.55	0.27	0.24	16.17	19.83	0.18	0.31	0.36	0.45	17.99	22.87	0.15	0.73	1.342	4312	1324	3412	
UGC 00891	40.7	12.50	1.00	105.48	109.80	1.20	0.74	0.71	0.355	34.69	39.01	0.37	0.31	0.85	0.484	36.69	43.17	0.37	0.34	0.91	0.54	38.08	46.72	0.44	0.40	2341	(234)1	2341	2341	
UGC 02259	43.7	1.94	0.929	48.19	52.51	0.59	0.33	2.87	0.991	53.77	58.08	0.42	0.39	0.13	0.013	39.18	45.66	0.36	0.45	0.04	0.003	40.71	49.34	0.35	0.53	3412	4321	1234	4312	
UGC 04325	43.7	0.73	0.355	44.97	49.76	0.29	0.30	1.09	0.64	47.49	52.28	0.28	0.43	0.24	0.038	43.31	50.49	0.28	0.34	0.21	0.041	44.89	54.47	0.27	0.38	1.324	4(23)1	1342	4312	
UGC 04699	54.7	0.73	0.355	44.97	49.76	0.29	0.30	1.09	0.64	47.49	52.28	0.28	0.43	0.24	0.038	43.31	50.49	0.28	0.34	0.21	0.041	44.89	54.47	0.27	0.38	1.324	4(23)1	1342	4312	
UGC 05716	41.1	18.53	1.000	211.76	217.70	1.57	1.18	1.81	0.946	44.55	50.49	0.42	0.19	2.01	0.966	46.54	55.45	0.42	0.25	2.26	0.979	48.54	60.42	0.42	0.25	2341	(234)1	2(34)1	2341	

SPARC Galaxies (Continue)																															
Statistics																															
Galaxy	$\delta$ Av	SCHIVE (1)					NFW (2)					SNFWDC (3)					SNFWC (4)					BEST MODEL									
		$\chi^2_{red}$	$P$ -Value	AIC	BIC	DIST	$\chi^2_{red}$	$P$ -Value	AIC	BIC	DIST	$\chi^2_{red}$	$P$ -Value	AIC	BIC	DIST	$\chi^2_{red}$	$P$ -Value	AIC	BIC	DIST	$\chi^2_{red}$	$P$ -Value	AIC	BIC	DIST	$B_{HIC}$	$B_{HST}$	$B_{HIC}$	$B_{HST}$	
DDO 161	58.4	0.31	0.00018	112.99	122.73	0.23	0.18	1.15	0.73	137.44	147.18	0.56	0.50	0.26	0.000027	113.36	127.97	0.23	0.14	0.27	0.000051	115.33	134.80	0.23	0.12	1342	(134)2	4312	3412	4312	3412
F 563-1	32.8	1.33	0.83	30413.27	30420.61	0.40	0.32	1.07	0.62	16230.84	16238.17	0.30	0.23	0.47	0.00001	2110.119	2112.19	0.27	0.16	0.40	0.028	21933.37	21948.04	0.26	0.16	2341	4321	(34)21	4321	4321	4321
F 563-2	34.8	0.00036	33183.54	33183.54	0.11	0.06	1.23	0.725	59093.79	59099.00	0.44	0.33	0.04	0.00009	38826.65	38836.46	0.13	0.09	0.0034	0.0	0.0034	39023.65	39034.07	0.12	0.12	1342	4321	1342	4312	4312	4312
F 568-1	36.1	0.16	0.00143	49621.16	49621.16	0.24	0.12	0.86	0.429	63319.03	63324.97	0.27	0.13	0.04	$5.0 \times 10^{-6}$	53300.01	53308.92	0.15	0.14	0.01	$2.0 \times 10^{-7}$	59085.67	59097.55	0.18	0.18	1342	3412	1234	4312	1234	4312
F 571-8	49.2	9.63	1.000	63193.52	63197.78	0.74	0.61	19.17	1.0000	54951.23	54957.40	1.20	0.93	10.59	1.00	63193.52	63202.91	0.74	0.61	10.80	1.00	62474.05	62486.57	0.62	0.67	2413	(13)42	(13)42	1342	1342	1342
F 579-1	46.5	1.78	0.955	29828.76	29835.32	0.52	0.37	0.19	0.00108	33342.86	33349.41	0.18	0.12	0.07	0.000013	32730.12	32739.95	0.17	0.15	0.02	$9.0 \times 10^{-8}$	32863.31	32876.42	0.17	0.12	1342	(34)21	(24)31	4321	4321	4321
NGC 1003	45.6	12.02	1.0000	550.57	560.90	1.20	0.93	2.57	1.000	229.02	239.36	0.45	0.31	2.65	1.000	231.03	246.53	0.45	0.28	1.17	0.767	183.19	203.86	0.33	0.18	4231	4(23)1	4321	4321	4321	4321
NGC 2915	33.5	0.95	0.46	209.11	218.71	0.39	0.20	0.96	0.47	209.31	218.92	0.39	0.27	0.49	0.0119	197.70	212.11	0.30	0.21	0.35	0.00090	195.63	214.84	0.26	0.26	3412	43(12)	1342	4312	4312	4312
NGC 2976	75.3	0.29	0.00021	126.89	136.08	0.23	0.22	1.90	0.9957	167.08	176.27	0.54	0.24	0.30	0.00041	128.89	142.67	0.23	0.22	0.31	0.00063	130.73	149.09	0.22	0.28	1342	4(13)2	(13)24	1342	1342	1342
NGC 4068	72.3	60.21	0.069	28.08	31.24	0.34	0.21	1.86	0.886	34.68	37.85	0.64	0.42	0.28	0.164	30.08	34.83	0.34	0.23	0.43	0.35	32.08	38.41	0.34	0.23	1324	(134)2	(134)2	1342	1342	1342
NGC 5585	54.1	5.11	1.000	193.74	202.45	0.44	0.32	7.17	1.0000	239.11	247.83	0.83	0.50	5.27	1.000	193.98	207.04	0.38	0.31	5.53	1.000	195.98	213.40	0.38	0.30	1342	(34)12	4312	1342	1342	1342
NGC 7793	66.2	1.05	0.62	309.46	320.78	0.21	0.14	0.89	0.32	302.45	313.76	0.31	0.21	0.81	0.195	300.12	317.10	0.30	0.20	0.81	0.199	301.35	323.98	0.30	0.20	2314	1(34)2	1(34)2	3412	3412	3412
UGC 01261	38.5	4.36	1.00	94.11	100.05	0.75	0.56	0.34	0.0295	53.92	59.86	0.20	0.12	0.11	0.00053	55.51	62.42	0.20	0.12	0.12	0.0017	55.51	67.39	0.20	0.16	2341	(234)1	(234)1	3421	3421	3421
UGC 01281	44.0	$4.6 \times 10^{-7}$	130.83	139.71	139.71	0.20	0.13	1.30	0.8478	157.46	166.34	0.37	0.32	0.15	$1.25 \times 10^{-6}$	132.83	146.14	0.20	0.13	0.10	$7.2 \times 10^{-8}$	133.73	151.48	0.20	0.08	1342	(134)2	4(13)2	4(13)2	4(13)2	4(13)2
UGC 04278	44.8	0.75	0.207	150.77	159.64	0.27	0.22	1.47	0.9324	167.28	176.16	0.43	0.37	0.53	0.038	147.19	160.51	0.28	0.21	0.80	0.279	154.29	172.04	0.27	0.21	1342	(14)32	(34)12	3142	3142	3142
UGC 04483	58.1	0.32	0.071	29.42	33.74	0.28	0.22	0.59	0.264	31.09	35.41	0.32	0.32	0.25	0.059	30.77	37.25	0.28	0.29	0.26	0.094	32.55	41.19	0.26	0.39	1234	4(13)2	1324	3412	3412	3412
UGC 05005	47.1	0.05	0.000017	78.33	83.92	0.24	0.18	0.22	0.0079	79.85	85.44	0.18	0.11	0.02	$2.0 \times 10^{-6}$	80.06	88.45	0.22	0.13	0.03	0.00002	82.06	93.25	0.22	0.13	1234	2(34)1	(34)12	3412	3412	3412
UGC 05414	60.5	0.23	0.079	26.71	29.88	0.31	0.27	1.05	0.619	29.98	33.14	0.37	0.36	0.11	0.044	28.11	32.86	0.30	0.37	0.15	0.14	30.10	36.43	0.30	0.49	1324	(34)12	1234	3412	1234	3412
UGC 05721	39.0	1.63	0.9655	154.41	162.95	0.48	0.35	0.96	0.49	140.45	148.90	0.37	0.20	0.46	0.0205	131.48	144.29	0.22	0.13	0.41	0.0119	132.06	149.14	0.19	0.13	3241	4321	(34)21	4321	4321	4321
UGC 05750	45.1	0.05	0.000021	69.98	75.58	0.18	0.22	1.00	0.57	78.57	84.16	0.25	0.16	0.04	0.00004	71.89	80.27	0.19	0.21	0.65	0.00013	73.85	85.04	0.18	0.15	1324	(14)32	4231	3(14)2	3(14)2	3(14)2
UGC 05829	48.1	0.47	0.105	64.12	69.71	0.27	0.16	0.09	0.00021	66.67	73.51	0.22	0.16	0.09	0.000024	62.21	70.60	0.20	0.17	0.02	0.00001	64.05	75.23	0.20	0.22	2134	2(34)1	(12)34	4321	4321	4321
UGC 06818	58.7	1.15	0.672	51.74	56.06	0.33	0.29	3.55	0.998	66.12	70.44	0.65	0.36	1.39	0.77	53.74	60.22	0.33	0.29	1.32	0.739	54.08	62.72	0.29	0.45	1342	4(13)2	(13)24	1432	1432	1432
UGC 06917	51.6	0.78	0.364	62.30	67.89	0.32	0.21	0.80	0.387	62.52	68.11	0.30	0.14	0.16	0.0046	58.60	66.99	0.20	0.23	0.07	0.0005	59.78	70.97	0.21	0.27	3124	3421	2134	4312	4312	4312
UGC 06923	66.2	0.31	0.126	36.20	39.37	0.33	0.31	0.95	0.57	38.80	41.96	0.36	0.35	0.41	0.253	38.20	42.95	0.33	0.33	0.18	0.17	39.34	45.67	0.28	0.59	1234	4(13)2	1324	4132	4132	4132
UGC 06983	46.6	1.39	0.9319	118.28	125.61	0.34	0.21	0.60	0.120	103.40	110.73	0.27	0.27	0.36	0.0156	101.55	112.55	0.23	0.28	0.34	0.0133	102.81	117.47	0.23	0.30	2341	(34)21	1234	4321	4321	4321
UGC 07089	62.0	0.24	0.0074	67.27	73.21	0.23	0.13	0.27	0.0119	67.57	73.51	0.22	0.16	0.12	0.00090	68.02	76.93	0.20	0.15	0.19	0.0070	70.38	82.26	0.21	0.14	1234	3421	1432	3412	3412	3412
UGC 07125	64.1	0.55	0.129	58.32	64.58	0.25	0.15	0.85	0.41	61.67	67.93	0.42	0.24	0.28	0.0146	57.10	66.49	0.23	0.13	0.31	0.029	59.10	71.62	0.23	0.14	1324	(34)12	1324	4132	4132	4132
UGC 07151	58.2	1.83	0.942	61.32	66.91	0.39	0.31	2.86	0.998	70.63	76.23	0.47	0.29	0.64	0.255	51.98	60.37	0.28	0.36	0.44	0.125	51.97	63.15	0.27	0.41	3412	4312	2134	4312	4312	4312
UGC 07232	62.4	0.11	0.11	21.13	22.67	0.22	0.26	2.41	0.911	25.73	27.28	0.54	0.27	0.09	0.23	22.99	25.31	0.19	0.52	-	-	25.13	28.22	0.22	0.43	1324	3(14)2	1243	312	312	312
UGC 07261	52.2	1.57	0.84	48.98	52.77	0.40	0.24	0.05	0.0014	41.38	45.16	0.20	0.13	0.06	0.007	43.38	49.05	0.20	0.14	0.03	0.006	45.21	52.78	0.19	0.27	2314	4(23)1	2314	4321	4321	4321
UGC 07323	64.2	0.35	0.053	52.22	57.43	0.20	0.11	0.71	0.1316	55.11	60.32	0.37	0.26	0.33	0.061	53.78	61.59	0.27	0.11	0.46	0.161	56.20	66.62	0.20	0.18	1234	(14)32	(13)42	3142	3142	3142
UGC 07559	62.2	0.05	0.0018	33.55	37.33	0.22	0.16	0.43	0.171	35.42	39.20	0.25	0.24	0.07	0.008	35.55	41.22	0.22	0.17	0.01	0.002	37.32	44.89	0.21	0.31	1234	4(13)2	1324	4132	4132	4132
UGC 07577	86.4	0.08	0.0008	41.86	46.65	0.22	0.08	0.20	0.0153	42.74	47.53	0.26	0.10	0.09	0.0029	43.86	51.05	0.22	0.08	0.11	0.010	45.86	55.44	0.22	0.08	1234	(134)2	(134)2	1342	1342	1342
UGC 07690	59.8	0.45	0.188	39.58	43.36	0.26	0.19	0.34	0.108	39.00	424																				